Programming Heteropolymetallic Lanthanide Helicates: Thermodynamic Recognition of Different Metal Ions Along the Strands

Solution and solid-state structures of $[Ln_3(L9)_3]^{9+}$

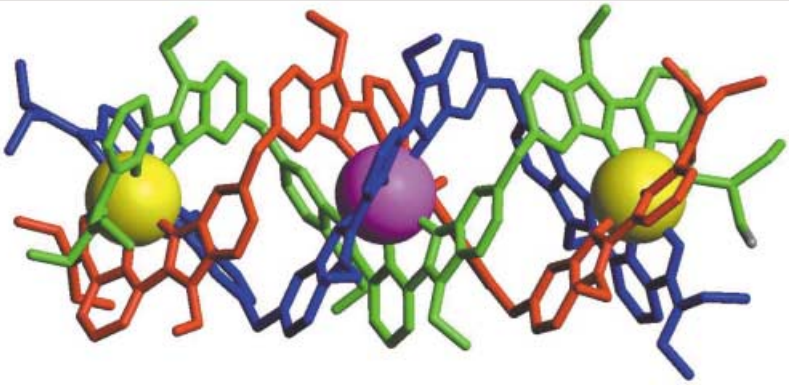

Thermodynamic model

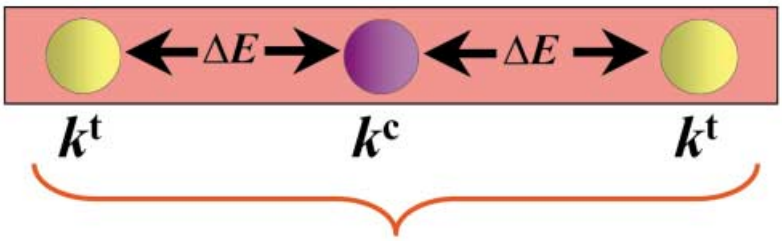

Absolute Affinities

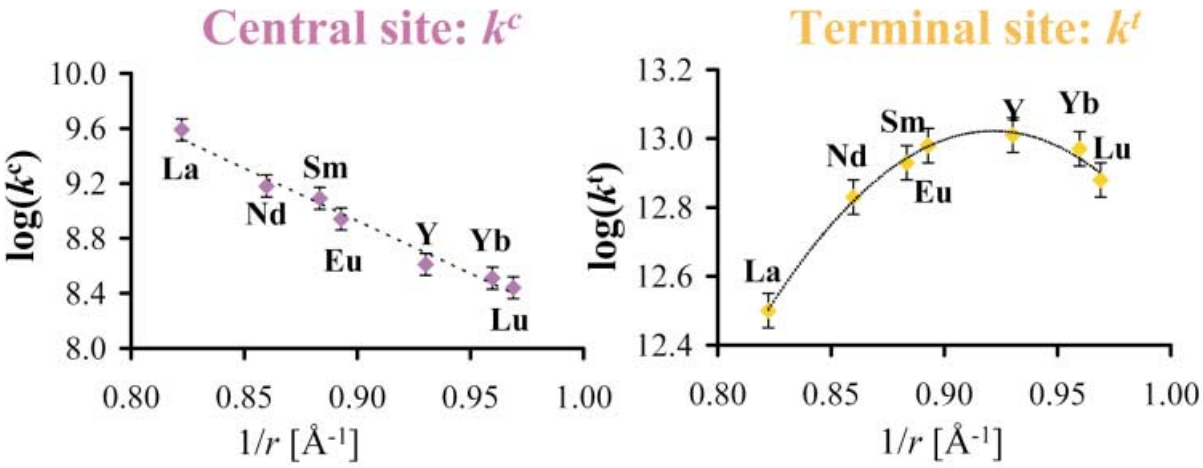

For more information see the following pages.

 DOI: 10.1002/chem.200305498

Programming Heteropolymetallic Lanthanide Helicates: Thermodynamic Recognition of Different Metal Ions Along the Strands

Sébastien Floquet,[a] Michal Borkovec,[a] Gérald Bernardinelli,[b] André Pinto,[c] Luc-Alexis Leuthold,[d] Gérard Hopfgartner,[d] Daniel Imbert,[e] Jean-Claude G. Bünzli,[e] and Claude Piguet*[a]

Abstract: Under stoichiometric conditions, the segmental tris-tridentate ligand L9 assembles with two different lanthanide metal ions Ln^1 and Ln^2 (Ln^1, Ln^2 = La, Nd, Sm, Eu, Yb, Lu, Y) to give mixtures of the heterotrimetallic triple-stranded helicates $[(Ln^1)_x(Ln^2)_{3-x}(L9)_3]^{9+}$ (x = 0–3) in acetonitrile. The combination of qualitative (ESI-MS) and quantitative (^{1}H NMR) speciations provides a set of thermodynamic data that were analysed with various statistical chemical models. A satisfying description requires the consideration of different affinities for the terminal N_6O_3 sites (k^t_{Ln}) and for the central N_9 site (k^c_{Ln}) for each specific lanthanide. The nontrivial dependence of these parameters on the ionic radius provides size-discriminating effects that favour the formation of heterotrimetallic helicates in which the central site is occupied by the larger metal of the pair. Combining the latter enthalpic driving forces with entropic contributions due to specific stoichiometric conditions allows partial selection (i.e., programming) of a specific heterotrimetallic species in solution, which can be isolated by crystallisation, as demonstrated for $[Eu_{2.04}La_{0.96}(L9)_3](CF_3SO_3)_9(CH_3NO_2)_9$ (**1**, $Eu_{2.04}La_{0.96}C_{207}H_{222}N_{48}O_{51}S_9F_{27}$, monoclinic, $P2_1/c$, Z = 4) in which the cation $[EuLaEu(L9)_3]^{9+}$ is the major component in the crystal. The scope and limitation of this approach is discussed together with the conditions for explicitly considering intermetallic interaction parameters u_{Ln1Ln2} in more sophisticated chemical models.

Keywords: helical structures · lanthanides · N ligands · thermodynamics

Introduction

Intermetallic communication between d- and f-block ions or between two different f-block ions can be exploited for inducing novel optical and magnetic properties in doped crystal lattices[1] and molecular solids.[2–5] As far as molecular programming is concerned, many efforts have focused on the design of pure heteropolymetallic d–f complexes, because the two different metal ions display clear-cut specific stereochemical preferences.[2,6] The related preparation of

[a] Dr. S. Floquet, Prof. Dr. M. Borkovec, Prof. Dr. C. Piguet
Department of Inorganic, Analytical and Applied Chemistry
University of Geneva, 30 quai E. Ansermet
1211 Geneva 4 (Switzerland)
Fax: (+4122) 379-6830
E-mail: Claude.Piguet@chiam.unige.ch

[b] Dr. G. Bernardinelli
Laboratory of X-ray crystallography
University of Geneva, 24 quai E. Ansermet
1211 Geneva 4 (Switzerland)

[c] A. Pinto
Department of Organic Chemistry
University of Geneva, 24 quai E. Ansermet
1211 Geneva 4 (Switzerland)

[d] L.-A. Leuthold, Prof. Dr. G. Hopfgartner
School of Pharmacy
Laboratory of Analytical Pharmaceutical Chemistry
University of Geneva, 20 bd d'Yvoy
1211 Geneva 4 (Switzerland)

[e] Dr. D. Imbert, Prof. Dr. J.-C. G. Bünzli
Institute of Molecular and Biological Chemistry
Swiss Federal Institute of Technology, BCH 1402
1015 Lausanne (Switzerland)

Supporting information for this article is available on the WWW under http://www.chemeurj.org/ or from the author. Table S1 lists the ESI-MS peaks, and Table S2 the ^{1}H NMR signals observed for mixtures of the heterotrimetallic complexes $[(Ln^1)_x(Ln^2)_{3-x}(L9)_3]^{9+}$ in acetonitrile. Tables S3 and S4 list experimental and S5 calculated mole fractions for the heterotrimetallic complexes obtained under different stoichiometric conditions. Table S6 collects structural data for the triple-helical cation in the crystal structure of $[La_{0.96}Eu_{2.04}(L9)_3](CF_3SO_3)_9(CH_3NO_2)_9$ (**1**). Figures S1 and S2 show ESI-MS and ^{1}H NMR spectra obtained for different stoichiometric ratios Ln^1:Ln^2:L9.

DOI: 10.1002/chem.200305498

heteropolymetallic f–f′ complexes is more challenging in view of the very similar coordination behaviour exhibited by the trivalent lanthanides Ln^{III} along the $4f^n$ series, except for a smooth and monotonous contraction on going from La ($4f^0$, $r_{La}^{CN=9}=1.216$ Å) to Lu ($4f^{14}$, $r_{Lu}^{CN=9}=1.032$ Å).[7] In this context, the isolation of heterometallic lanthanide-containing molecular materials in the solid state that display significant deviations from the expected statistical distribution has attracted much attention during the last decade with the detailed investigations of the Schiff bases L1[4a] and L2,[4b] and the macrocyclic ligands L3,[5a,b] L4[5c,d] and L5.[4c] Interestingly, L5 selectively produces pentametallic lanthanide clusters

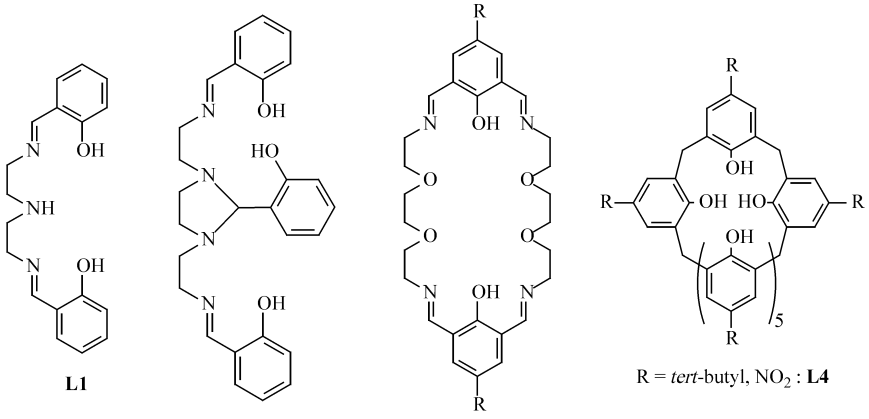

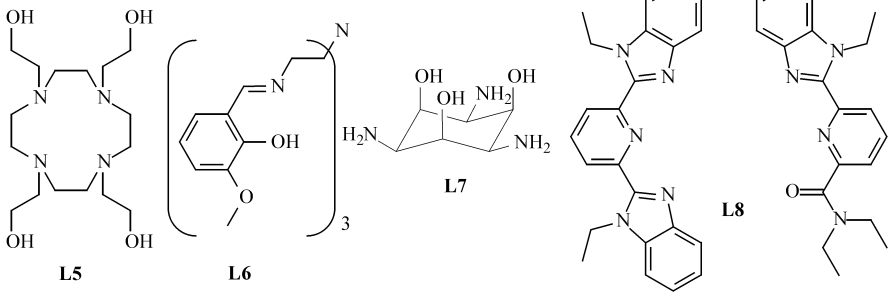

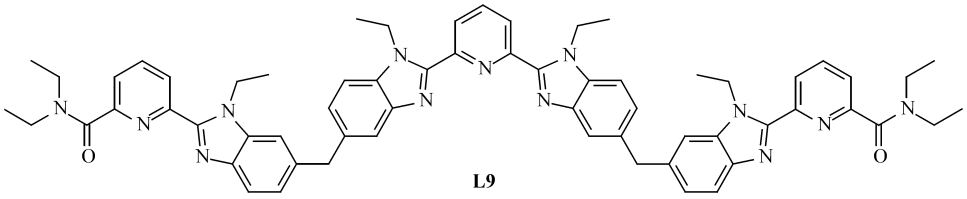

$[Ln_5(\mu_4\text{-L5})](NO_3)_6(\mu_5\text{-OH})]$ in which the metal ions are distributed among two different sites. The introduction of a mixture of lanthanides Ln^1 and Ln^2 results in nonstatistical enrichments, which are diagnostic for cooperative, multimetal-recognition processes, but the two-step procedure leading to the heterometallic complexes in the solid phase (thermodynamic equilibrium in solution followed by a thermodynamically and/or kinetically controlled crystallisation process) prevents a direct access to the parameters governing the selective incorporation of different Ln^{III} ions.[4c]

A deeper understanding of the recognition processes leading to pure heterobimetallic f–f′ complexes requires their formation in solution under kinetic or thermodynamic control. The former case is illustrated by the inert triple-decker sandwich complexes $[(Por)Ln^1(Pc)Ln^2(Por)]$, $[(Pc)Ln^1(Por)Ln^2(Pc)]$, $[(Pc)Ln^1(Pc)Ln^2(Por)]$ and $[(Pc)Ln^1(Pc)Ln^2(Pc^*)]$, in which the porphyrin (Por) or phthalocyanine (Pc) macrocycles coordinate to two different Ln^{III} atoms according to a stepwise strategy.[3d,e] The alternative thermodynamic approach is probably responsible for the surprising isolation of the first pure heterobimetallic LaYb complex $[LaYb(L6)(acetone)(NO_3)_2]_2[La(NO_3)_5(H_2O)]$,[3a] as demonstrated by a rational extension of this synthesis leading to 91 different heterometallic compounds in which the smaller lanthanide of any Ln^1/Ln^2 pair selectively occupies the inner N_4O_3 cavity.[3b] Although no direct evidence supports the persistence of the heterobimetallic structures in solution, FABMS experiments using DMF as solvent and *m*-NBA as matrix suggest similar formulations in solution.[3b] However, unambiguous thermodynamic f–f′ recognition has been rarely established in solution, and a recent potentiometric investigation on the formation of the neutral heterotrimetallic sandwich complexes $[(Ln^1)(Ln^2)_2(L7\text{-}3H)_2(H_2O)_6]^{3+}$ and $[(Ln^1)(Ln^2)(Ln^3)(L7\text{-}3H)_2(H_2O)_6]^{3+}$ in water shows only minor deviations from the statistical distribution.[8,9] The design of different metal-hosting sites is an obvious solution for increasing selectivity, and Bünzli et al. have reported the formation of the heterobimetallic C_3-symmetrical head-to-head-to-head triple-stranded helicates *HHH*-$[(Ln^1)(Ln^2)(L8)_3]^{6+}$, in which the smaller lanthanide occupies the N_6O_3 cavity.[10] The equilibrium $[(Ln^1)_2(L8)_3]^{6+} + [(Ln^2)_2(L8)_3]^{6+} \rightleftarrows 2[(Ln^1)(Ln^2)(L8)_3]^{6+}$ is systematically displaced to the right with respect to its statistical value, and an increasing difference in ionic radii favours the formation of the heterobimetallic complex.[10] For the La/Lu pair, this translates into the formation of 90% of the heterobimetallic helicate *HHH*-$[(La)(Lu)(L8)_3]^{6+}$ at millimolar concentrations, but the potential coexistence of *HHH* and *HHT* (head-to-head-to-tail) isomers limits the selectivity of the assembly process for other similar ligands.[11] This limitation is removed for the C_{2v}-symmetrical tris-tridentate ligand L9: its self-assembly with Ln^{III} gives D_3-symmetrical homotrimetallic helicates $[Ln_3(L9)_3]^{9+}$ existing as single isomers with

different terminal (N_6O_3) and central (N_9) coordination sites.[12] Here we report an investigation on the thermodynamic assembly process leading to the heterotrimetallic complexes $[(Ln^1)_2(Ln^2)(L9)_3]^{9+}$ and $[(Ln^1)(Ln^2)_2(L9)_3]^{9+}$. Particular attention is focused on the development of a predictive thermodynamic model rationalising specific recognition processes at the two different sites, which have no counterpart in analogous monometallic triple-helical complexes or podates.

Results and Discussion

All experiments were performed under stoichiometric conditions, that is, $[Ln]_{tot}:[L9]_{tot}=3:3$, while the ratio $Ln^1:Ln^2$ was varied. For the sake of simplicity, homotrimetallic helicates $[Ln_3(L9)_3]^{9+}$ are designated by Ln_3 and heterotrimetallic species $[(Ln^1)_x(Ln^2)_{3-x}(L9)_3]^{9+}$ by $Ln^1{}_xLn^2{}_{3-x}$; where necessary, the location of Ln^{III} in the three different sites in the helicates is given in the order terminal site (t), central site (c), terminal site (t); for example, $Ln^1Ln^2Ln^1$ represents a helicate in which Ln^1 ions occupy the terminal sites, and Ln^2 the central site.

Speciation and formation constants for diamagnetic and weakly paramagnetic homo- and heterotrimetallic (Ln^1, Ln^2 = La, Sm, Lu, Y) helicates: According to the formation constants previously reported for the assembly of a single type of Ln^{III} with L9 in acetonitrile (Ln = La–Lu),[12] homotrimetallic complexes Ln_3 account for more than 98% of the ligand speciation under stoichiometric conditions and for $[L9]_{tot} \geq 5\times10^{-4}$ M. Therefore, under the same experimental conditions, reaction of L9 with two different lanthanide triflates produces exclusively two homotrimetallic complexes $(Ln^1)_3$, $(Ln^2)_3$ and four heterotrimetallic species $Ln^1Ln^1Ln^2$, $Ln^1Ln^2Ln^1$, $Ln^2Ln^2Ln^1$ and $Ln^2Ln^1Ln^2$ in significant quantities (Figure 1).

A reliable qualitative speciation for $[L9]_{tot}=5\times10^{-4}$ M was obtained by ESI-MS for different $Ln^1:Ln^2$ ratios (3:0, 2:1, 1.5:1.5, 1:2 and 0:3). We systematically observe a series of peaks corresponding to $[(Ln^1)_x(Ln^2)_{3-x}(L9)_3(CF_3SO_3)_n]^{(9-n)+}$ species with $n=1$–6 (Figure 2a). For each value of n, we detect four patterns originating from each possible value of $x=0$, 1, 2, 3 (Figure 2b and Table S1, Supporting Information). Some minor residual peaks in the ESI-MS spectra arise from traces of protonated ligands and from partial hydrolysis of the terminal carboxamide groups during the spraying process. We conclude that the expected homo- and heterotrimetallic helicates are the only significant complexes in solution under these experimental conditions.

Although the varying efficiency of transfer of the cations from the droplet into the gas phase for complexes with different charges (i.e., different n) prevents quantitative comparisons with ESI-MS,[13] a reliable speciation can be obtained for the structurally related helicates $[(Ln^1)_x(Ln^2)_{3-x}(L9)_3(CF_3SO_3)_n]^{(9-n)+}$ with the same n, as recently demonstrated for monometallic triple-helical lanthanide complexes[14] and for heterobimetallic helicates with L8.[10] Any variation of the relative intensity of the ESI-MS signal within a tetrad can thus be assigned to a concomitant change in the speciation in solution (Figure S1, Supporting Information), and it is noteworthy that we systematically observe significant deviations from the statistical binomial distribution $(Ln^1)_3:(Ln^1)_2Ln^2:Ln^1(Ln^2)_2:(Ln^2)_3=1:3:3:1$ for mixtures with $Ln^1:Ln^2=1.5:1.5$ (Figure 2b). This suggests that the central N_9 site and the terminal N_6O_3 sites display different affinities for the lanthanide ions, but further interpretation is precluded because the relative quantities of $Ln^1Ln^1Ln^2$ versus $Ln^1Ln^2Ln^1$ or $Ln^2Ln^2Ln^1$ versus $Ln^2Ln^1Ln^2$ cannot be evaluated by mass spectrometry. We thus resorted to ^{1}H NMR spectroscopy for determining the relative quantities of the six helicates shown in Figure 1 for various $Ln^1:Ln^2$ ratios and $[L9]_{tot}=10^{-2}$ M. Under these conditions, we systematically detect exclusive formation of the triple-stranded helicates (no trace of hydrolysis), and Figure 3 shows the evolution of the ^{1}H NMR spectra for different La/Lu mixtures from which the spectrum of each individual

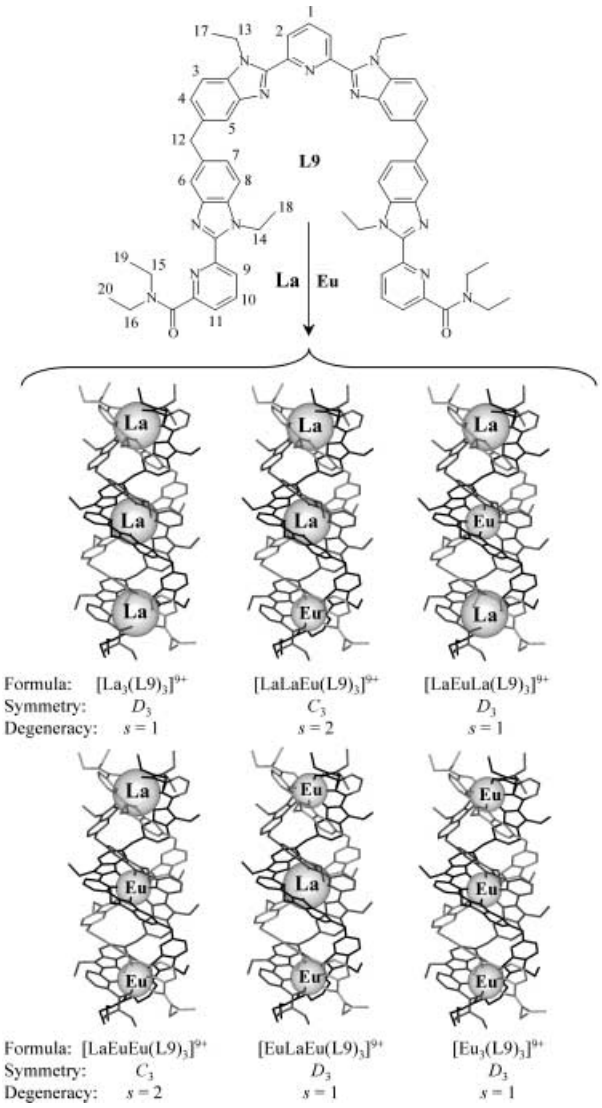

Figure 1. Schematic representation of the assembly process of L9 with the La/Eu pair leading to the homotrimetallic complexes $[La_3(L9)_3]^{9+}$ and $[Eu_3(L9)_3]^{9+}$ and the heterotrimetallic complexes $[LaLaEu(L9)_3]^{9+}$, $[LaEuLa(L9)_3]^{9+}$, $[LaEuEu(L9)_3]^{9+}$ and $[EuLaEu(L9)_3]^{9+}$.

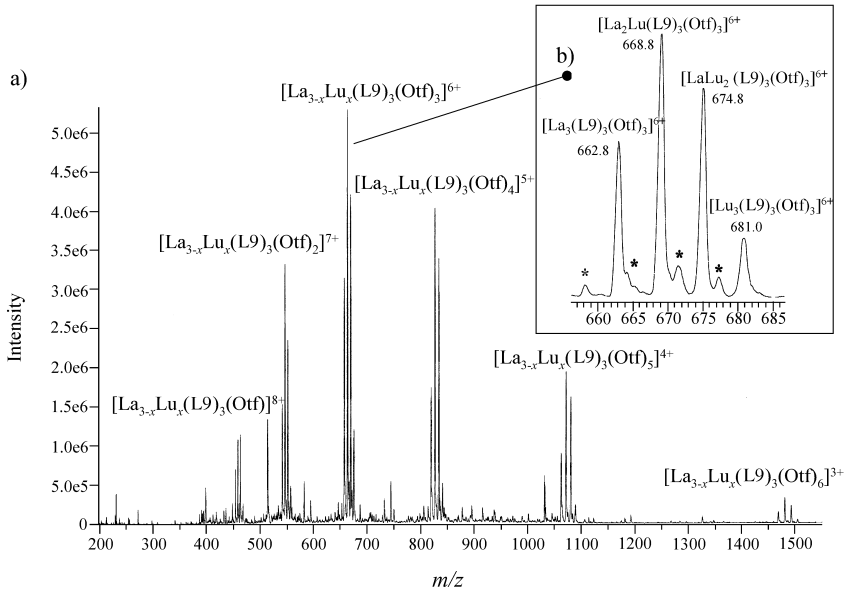

Figure 2. a) ESI-MS spectrum obtained for a mixture of L9 (3 equiv, $5\cdot10^{-4}$ M) with $La(CF_3SO_3)_3$ (1.5 equiv) and $Lu(CF_3SO_3)_3$ (1.5 equiv) in acetonitrile, showing the adduct ions $[(La)_{3-x}(Lu)_x(L9)_3(CF_3SO_3)_n]^{(9-n)+}$ ($n=1$–6). b) Part of the ESI-MS spectrum for $n=3$; * corresponds to analogous complexes in which one terminal carboxamide is hydrolysed, $Otf^- = CF_3SO_3^-$).

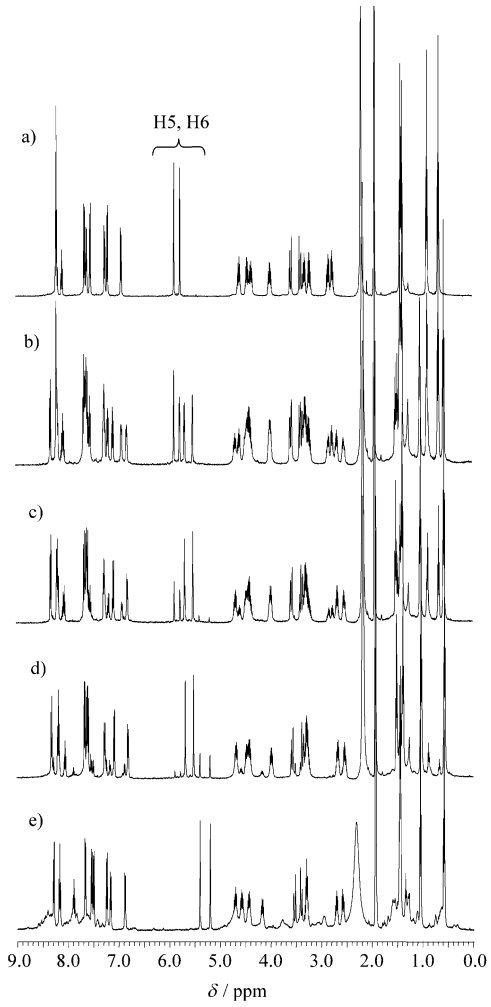

Figure 3. ^{1}H NMR spectra recorded at 500 MHz for different La:Lu ratios in CD_3CN ($[L9]_{tot}=10^{-2}$ M, $[Ln]_{tot}$:$[L9]_{tot}=3$:3, 298 K): La:Lu = a) 3:0, b) 2:1, c) 1.5:1.5, d) 1:2, e) 0:3.

complex and its relative quantity can be obtained by 1) thorough analysis of the number and multiplicity of the proton resonances (by means of {^{1}H-^{1}H}-COSY) and {^{1}H-^{1}H}-NOESY correlation spectra) and 2) careful integration of the ^{1}H NMR signals for the different complexes. For diamagnetic (La, Lu, Y) or weakly paramagnetic (Sm) lanthanides, the analysis mainly focuses on protons H5 and H6 (see Figure 1). The latter display isolated singlets, broadened by the unresolved aromatic ^4J scalar coupling, in an unusual spectral range (5.0–6.0 ppm) in view of the specific diamagnetic anisotropy produced by the benzimidazole groups of the neighbouring wrapped ligand strands (Figure 3).[12]

The signals of the homotrimetallic $(Ln^1)_3$ and $(Ln^2)_3$ helicates are easily assigned by comparison with pure samples (Figure 4a and e), whilst those of the heterotrimetallic complexes are ascribed to the remaining signals according to 1) their symmetry (C_3-symmetrical $Ln^1Ln^1Ln^2$ and $Ln^2Ln^2Ln^1$ exhibit four signals of equal intensity, while D_3-symmetrical $Ln^1Ln^2Ln^1$ and $Ln^2Ln^1Ln^2$ generate two signals) and 2) their evolution with changing Ln^1:Ln^2 ratio (Figure 4b–d). The resulting picture is in entire agreement with ESI-MS data. Further scalar and dipolar correlations allow the complete analysis of the ^{1}H NMR data (Table S2, Supporting Information), while careful integrations of the signals provide reliable relative concentrations for each complex (Table 1; Tables S3, S4, Supporting Information).

Interestingly, we observe for the five pairs La/Lu, La/Y, La/Sm, Sm/Lu and Sm/Y (whereby Ln^1 is the larger Ln) that the C_3-symmetrical $Ln^1Ln^2Ln^2$ and D_3-symmetrical $Ln^1Ln^2Ln^1$ helicates, in which the central site is occupied by the smaller lanthanide, are systematically less stable than the other complexes, and thus appear as minor species under our experimental conditions (Table 1). Substantial overlap of the H5 and H6 signals prevents determination of the speciation for Y/Lu. Taking the $\log(\beta_{33}^{Ln})$ values determined by spectrophotometry for the Ln_3 helicates as initial estimations, the formation constants for each homo- [$\log(\beta_{33}^{Ln,exptl})$, Eq. (1)] and heterotrimetallic helicate [$\log(\beta_{33}^{Ln^jLn^kLn^l,exptl}$, Eq. (2)] observed in solution can be adjusted with the program MINEQL$^+$[15] by fitting their relative experimental ratios determined by ^{1}H NMR spectroscopy for different Ln^1:Ln^2 ratios (Table 1; Tables S3 and S4, Supporting Information). Within experimental error, identical $\log(\beta_{33}^{Ln,exptl})$ are obtained for the same homotrimetallic complexes contributing in different pairs (e.g., $\log(\beta_{33}^{La,exptl})$ deter-

Table 1. Mole fractions of homo- and heterotrimetallic helicates $[(Ln^1)_x(Ln^2)_{3-x}(L9)_3]^{9+}$ ($x=0$, 1, 2, 3) observed by ^{1}H NMR spectroscopy in CD_3CN for Ln^1:Ln^2:L9 = 1.5:1.5:3 ($[L9]_{tot}=10^{-2}$ M, 298 K).

Ln^1	Ln^2	Δr_i [Å][a]	$[Ln^1_3L_3]^{9+}$	$[Ln^1Ln^2Ln^1L_3]^{9+}$	$[Ln^1Ln^1Ln^2L_3]^{9+}$	$[Ln^2Ln^1Ln^2L_3]^{9+}$	$[Ln^1Ln^2Ln^2L_3]^{9+}$	$[Ln^2_3L_3]^{9+}$	$\Delta G^{exptl}_{[Eq.\ (6)]}$ [kJ mol^{-1}]
La	Lu	0.184	0.13	< 0.01	0.39	0.44	< 0.01	0.04	−8.9
La	Yb	0.174	0.04	< 0.01	0.23	0.56	0.14	0.03	−11.9
La	Y	0.141	0.07	< 0.01	0.36	0.51	0.03	0.04	−10.3
Nd	Lu	0.131	0.10	0.03	0.37	0.38	0.04	0.08	−7.7
Sm	Lu	0.100	0.13	< 0.01	0.36	0.41	0.06	0.04	−8.4
La	Eu	0.096	0.04	< 0.01	0.32	0.58	< 0.01	0.07	−10.5
Eu	Lu	0.088	0.19	0.06	0.43	0.23	0.07	0.02	−9.1
La	Sm	0.084	0.08	< 0.01	0.37	0.46	< 0.01	0.10	−7.6
Sm	Y	0.057	0.12	< 0.01	0.39	0.35	0.05	0.10	−6.4
Y	Lu	0.043	–	–	–	–	–	–	–

[a] $\Delta r_i = r_{Ln1} - r_{Ln2}$ for nine-coordinate ionic radii taken from reference [22].

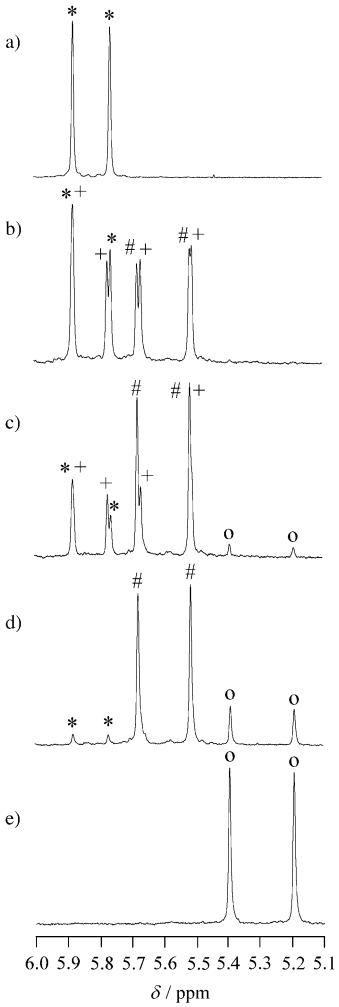

Figure 4. Part of the ^{1}H NMR spectra highlighting the signals of protons H5 and H6 for different La:Lu ratios in CD_3CN ($[L9]_{tot}=10^{-2}$ M, $[Ln]_{tot}$:$[L9]_{tot}$ = 3:3, 298 K): La:Lu = a) 3:0, b) 2:1, c) 1.5:1.5, d) 1:2, and e) 0:3. * = $[La_3(L9)_3]^{9+}$, + = $[LaLaLu(L9)_3]^{9+}$, # = $[LuLaLu(L9)_3]^{9+}$, ○ = $[Lu_3(L9)_3]^{9+}$.

mined for the La/Y, La/Sm or La/Lu pairs). The formation constants are collected in Table 2.

$$3\,Ln^{3+} + 3\,L9 \rightleftharpoons [Ln_3(L9)_3]^{9+} \quad \log(\beta_{33}^{Ln,exptl}) \tag{1}$$

$$[Ln^i]^{3+} + [Ln^k]^{3+} + [Ln^l]^{3+} + 3\,L9 \rightleftharpoons [Ln^iLn^kLn^l(L9)_3]^{9+} \quad \log(\beta_{33}^{Ln^iLn^kLn^l,exptl}) \tag{2}$$

Speciation and formation constants for paramagnetic homo- and heterotrimetallic helicates: To substantiate possible recognition processes in the triple-stranded helicates occurring along the lanthanide series, ultrafast-relaxing paramagnetic trivalent ions with representative ionic sizes were selected (Ln^1 = Nd, Eu, Yb) for investigating the formation constants of additional heterotrimetallic complexes with Ln^2 = La, Lu. Although paramagnetic shifts improve the separation of the ^{1}H NMR signals originating from the different complexes in equilibria, the concomitant contribution of the electron-induced nuclear relaxation limits the detection of intramolecular {^{1}H-^{1}H} scalar and {^{1}H-^{1}H} dipolar interactions. Moreover, the significant contact and pseudocontact shifts observed for H5 and H6[16] complicate 1) their straightforward assignment in heterotrimetallic helicates and 2) quantitative analysis of the speciation in solution (Figure S2, Supporting Information). We thus resorted to the detailed model-free analysis of paramagnetic ^{1}H NMR data previously applied to the homotrimetallic complexes for the, a priori, calculation of paramagnetic ^{1}H NMR shifts for the heterotrimetallic species.[16] The chemical shift δ^{exptl}_{ijkl} of a proton i in $Ln^jLn^kLn^l$ is given by Equation (3), in which δ^{dia}_i is the diamagnetic shift measured in the analogous homotrimetallic La, Y or Lu complex, $F_i\langle S_z\rangle_{j,k,l}$ is the through-bond contact shift limited to a single site (j, k or l), and $C_kB_0^{2^{central1}}G_i^1 + C_jB_0^{2^{terminal2}}G_i^2 + C_lB_0^{2^{terminal3}}G_i^3$ are the three additive through-space pseudocontact contributions induced by the three paramagnetic ions.[16,17]

$$\delta^{exptl}_{ijkl} = \delta^{dia}_i F_i\langle S_z\rangle_{j,k,l} + C_kB_0^{2^{central1}}G_i^1 + C_jB_0^{2^{terminal2}}G_i^2 + C_lB_0^{2^{terminal3}}G_i^3 \tag{3}$$

If we consider the crystal structure of $[Eu_3(L9)_3]^{9+}$ to be an acceptable structural model for homo- and heterotrimetallic helicates in solution along the complete lanthanide series,[12] we can use the set of contact terms F_i (i.e., Fermi constants), structural factors G_i^n (n = 1–3) and crystal-field parameters reported for the homotrimetallic helicates ($B_0^{2^{central}}$(Ce-Tb) = −45, $B_0^{2^{central}}$(Dy-Yb) = −33, $B_0^{2^{terminal}}$(Ce-Tb) = −67 and $B_0^{2^{terminal}}$(Dy-Yb) = −61 ppm Å^3)[16] for calculating the ^{1}H NMR spectra of the heterotrimetallic complexes with Equation (3). For instance, δ^{exptl}_{ijkl} for D_3-symmetrical YbLaYb can be predicted with simplified Equation (4), while that of LuNdLu can be predicted with the simplified

Table 2. Experimental $\log(\beta_{33}^{Ln,exptl})$ and calculated $\log(\beta_{33}^{Ln,calcd})$ formation constants for the complexes $[(Ln^1)_x(Ln^2)_{3-x}(L9)_3]^{9+}$ ($x=0$, 1, 2, 3) observed by ^{1}H NMR spectroscopy in CD_3CN at 298 K.

Ln^1, Ln^2	Compound	$\log(\beta_{33}^{Ln,exptl})$ NMR[a]	$\log(\beta_{33}^{Ln,calcd})\pm0.1$ Model B	Model C	Ln^1, Ln^2	Compound	$\log(\beta_{33}^{Ln,exptl})$ NMR[a]	$\log(\beta_{33}^{Ln,calcd})\pm0.1$ Model B	Model C
La, –	La_3	34.6 ± 0.2	–	34.6	Nd, Lu	LuNdLu	35.2 ± 0.1	34.4	35.0
		34.3 ± 1.2[b]	–		0.131[e]	NdLuLu	34.4 ± 0.1	34.7	34.4
Nd, –	Nd_3	34.8 ± 0.1	–	34.8	Sm, Lu	SmLuSm	–	34.7	34.3
		35.0 ± 1.1[b]	–		0.100[e]	SmSmLu	35.4 ± 0.1	35.0	35.2
Sm, –	Sm_3	35.0 ± 0.1	–	35.0		LuSmLu	35.3 ± 0.1	34.5	34.9
Eu, –	Eu_3	34.9 ± 0.1	–	34.9		SmLuLu	34.5 ± 0.1	34.8	34.6
		34.8 ± 1.6[b]	–		La, Eu	LaEuLa	–	34.7	33.9
Y, –	Y_3	34.7 ± 0.1	–	34.6	0.096[e]	LaLaEu	35.4 ± 0.1	35.0	35.4
		35.0 ± 1.2[b, c]	–			EuLaEu	35.6 ± 0.1	34.8	35.5
Yb, –	Yb_3	34.4 ± 0.1	–	34.5		LaEuEu	–	35.1	34.7
		34.5 ± 1.8[b, d]	–		Eu, Lu	EuLuEu	34.6 ± 0.2	34.7	34.4
Lu, –	Lu_3	34.2 ± 0.3	–	34.2	0.088[e]	EuEuLu	35.4 ± 0.2	35.0	35.1
		33.9 ± 0.3[b]	–			LuEuLu	35.0 ± 0.2	34.4	34.7
La, Lu	LaLuLa	–	34.5	33.4		EuLuLu	34.4 ± 0.2	34.7	34.6
0.184[e]	LaLaLu	35.3 ± 0.1	34.8	35.3	La, Sm	LaSmLa	–	34.7	34.1
	LuLaLu	35.3 ± 0.1	34.3	35.3	0.084[e]	LaLaSm	35.2 ± 0.1	35.0	35.3
	LaLuLu	–	34.6	34.1		SmLaSm	35.6 ± 0.1	34.9	35.5
La, Yb	LaYbLa	–	34.5	33.5		LaSmSm	–	35.2	34.8
0.174[e]	LaLaYb	35.2 ± 0.1	34.8	35.4	Sm, Y	SmYSm	–	34.9	34.5
	YbLaYb	35.6 ± 0.1	34.5	35.5	0.057[e]	SmSmY	35.4 ± 0.1	35.2	35.3
	LaYbYb	34.4 ± 0.1	34.8	34.3		YSmY	35.3 ± 0.1	34.8	35.1
La, Y	LaYLa	–	34.6	33.6		SmYY	34.5 ± 0.1	35.1	34.8
0.141[e]	LaLaY	35.4 ± 0.1	34.9	35.4	Y, Lu	YLuY	–	34.5	34.5
	YLaY	35.6 ± 0.1	34.7	35.6	0.043[e]	YYLu	–	34.8	34.8
	LaYY	34.4 ± 0.1	35.0	34.4		LuYLu	–	34.4	34.4
Nd, Lu	NdLuNd	34.2 ± 0.1	34.6	34.1		YLuLu	–	34.7	34.6
0.131[e]	NdNdLu	35.2 ± 0.1	34.9	35.2					

[a] Determined from the fit of NMR data (see text). [b] Obtained by direct spectrophotometric titrations of L9 with Ln^{III}, from ref. [12]. [c] Measured for Ln = Ho, which has a very similar ionic radius.[12] [d] Measured for Ln = Tm, which has a very similar ionic radius.[12] [e] $\Delta r_i = r_{Ln1} - r_{Ln2}$ [Å]: nine-coordinate ionic radii taken from reference [22].

Equation (5), because the Bleaney factors vanish for diamagnetic ions ($C_{La} = C_{Lu} = 0$).[17]

$$\delta_{i\mathrm{YbLaYb}}^{\mathrm{calcd}} = \delta_{i\mathrm{LuLaLu}}^{\mathrm{dia}} + F_i^{\mathrm{terminal}}\langle S_z\rangle_{\mathrm{Yb}} + C_{\mathrm{Yb}}B^{2\,\mathrm{terminal}}_{0_{\mathrm{Ln=Dy-Yb}}}(G_i^2 + G_i^3) \quad (4)$$

$$\delta_{i\mathrm{LuNdLu}}^{\mathrm{calcd}} = \delta_{i\mathrm{LuLaLu}}^{\mathrm{dia}} + F_i^{\mathrm{central}}\langle S_z\rangle_{\mathrm{Nd}} + C_{\mathrm{Nd}}B^{2\,\mathrm{central}}_{0_{\mathrm{Ln=Ce-Tb}}}G_i^1 \quad (5)$$

Good correlations are obtained between calculated and experimental ^{1}H NMR data for each heterotrimetallic complex, and thus lead to complete assignment of their signals (Table 3; Table S2, Supporting Information). Subsequent integrations of the signals provide a reliable speciation (Table 1; Tables S3, S4, Supporting Information); this eventually leads to stability constants for the La/Eu, Nd/Lu, Eu/Lu and La/Yb pairs (Table 2) and confirms the preferred location of the smaller Ln^{III} of the pair in the terminal sites (Table 1).

Modelling the thermodynamic assembly of heterotrimetallic helicates $(Ln^1)_x(Ln^2)_{3-x}$ (Ln^1, Ln^2 = La, Nd, Sm, Eu, Yb, Lu, Y; x = 1, 2): A straightforward model considers the triple-stranded trimetallic helicates as receptors made up of three wrapped strands defining two terminal nine-coordinate N_6O_3 sites and one central nine-coordinate N_9 site with respective absolute affinities k_{Ln}^t and k_{Ln}^c reflecting the specific free energy of complexation for each site (i.e., $\log(k_{Ln}^t)$ and $\log(k_{Ln}^c)$ are proportional to ΔG, Scheme 1). At the concentrations used for NMR studies, no significant decomplexation occurs, and the stoichiometric ratio used ensures that the three sites are quantitatively occupied by Ln^{III} ions. Interactions between a pair of adjacent metal atoms (electrostatic repulsion, mechanical coupling) is modelled by a single free-energy term ΔE, expressed as a Boltzmann factor $u_{Ln1Ln2} = \exp(-\Delta E_{Ln1Ln2}/RT)$, as previously described for multiple protonation or complexation processes (Scheme 1).[18]

Table 3. Experimental δ_{ijkl}^{exptl} and calculated δ_{ijkl}^{calcd} ^{1}H NMR shifts for selected paramagnetic heterotrimetallic complexes $[LnLaLn(L9)_3]^{9+}$ [Eq. (4)] and $[LuLnLu(L9)_3]^{9+}$ [Eq. (5)] in CD_3CN at 298 K (numbering in Figure 1).

Compound		H1	H2	H3	H4	H5	H6	H7	H8	H9	H10	H11	Me17	Me18	Me19	Me20
$[EuLaEu(L9)_3]^{9+}$	$\delta_{i\mathrm{EuLaEu}}^{exptl}$	8.67	8.47	8.19	7.70	8.84	10.99	7.35	5.86	4.14	6.00	4.89	2.00	0.11	0.42	3.51
	$\delta_{i\mathrm{EuLaEu}}^{calcd}$	8.44	8.07	7.49	7.14	7.04	14.81	7.90	4.89	4.31	6.80	5.32	1.68	1.01	0.40	3.05
$[YbLaYb(L9)_3]^{9+}$	$\delta_{i\mathrm{YbLaYb}}^{exptl}$	9.41	9.52	9.11	8.41	12.77	19.36	7.70	6.68	5.28	5.13	3.75	2.70	−1.75	−0.15	7.53
	$\delta_{i\mathrm{YbLaYb}}^{calcd}$	9.96	9.88	9.10	8.41	12.79	19.50	8.77	7.17	3.17	5.07	4.34	2.92	−1.10	−0.89	7.22
$[LuNdLu(L9)_3]^{9+}$	$\delta_{i\mathrm{LuNdLu}}^{exptl}$	9.83	10.38	8.68	7.18	−0.06	3.41	6.57	6.75	7.90	7.90	7.36	2.50	1.13	0.83	0.31
	$\delta_{i\mathrm{LuNdLu}}^{calcd}$	9.58	10.46	7.75	6.61	0.69	4.66	7.18	7.43	8.12	8.05	7.51	1.64	1.58	0.90	0.44
$[LuEuLu(L9)_3]^{9+}$	$\delta_{i\mathrm{LuEuLu}}^{exptl}$	5.71	3.50	5.80	7.33	10.86	7.55	7.15	7.59	8.72	8.44	7.96	1.70	0.44	1.26	0.84
	$\delta_{i\mathrm{LuEuLu}}^{calcd}$	5.45	2.21	5.81	7.27	13.06	6.66	7.36	7.74	8.48	8.32	7.79	1.42	1.22	1.12	0.70

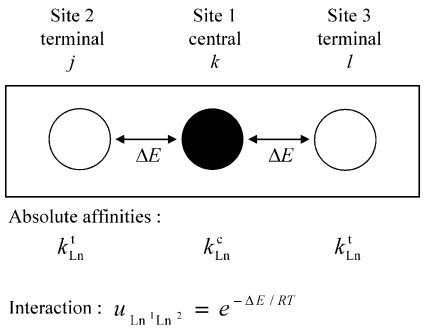

Scheme 1. Schematic representation of the triple-stranded helicates $[Ln_3(L9)_3]^{9+}$ used for thermodynamic modelling.

Model A—a simple statistical binomial distribution: The least sophisticated model considers that both the terminal and central sites display identical absolute affinities, which do not vary along the lanthanide series ($k^t_{Ln}=k^c_{Ln}=k$). Moreover, the interaction between adjacent sites is identical for any pair along the lanthanide series. Under these conditions, the speciation of $(Ln^1)_x(Ln^2)_{3-x}$ ($x=0$–3) in solution at $[L9]_{tot}=10^{-2}$ M follows a statistical binomial distribution that depends on the Ln^1:$Ln^2=p_1$:p_2 ratio ($p_1+p_2=1.0$). We expect the following distribution for the mole fraction of each specific helicate: $X((Ln^1)_x(Ln^2)_{3-x})=s(p_1)^x(p_2)^{(3-x)}$, in which s is the degeneracy given in Figure 1. This translates into $X(Ln^1)_3=X(Ln^2)_3=X(Ln^1Ln^2Ln^1)=X(Ln^2Ln^1Ln^2)=0.125$ and $X(Ln^1Ln^1Ln^2)=X(Ln^2Ln^2Ln^1)=0.25$ for a mixture containing equal quantities of Ln^1 and Ln^2 (i.e., $p_1=p_2=0.5$). Comparison with the experimental distributions obtained for Ln^1:$Ln^2=1.5$:1.5 (Table 1) shows only poor correlations, mainly resulting from the reluctance of the smaller lanthanide of each pair (Ln^2) to occupy the central site. Interestingly, the formation of the heterotrimetallic helicates according to global Equation (6) is systematically favoured, with $-11.9\,kJ\,mol^{-1}\le\Delta G^{exptl}_{[Eq.\,(6)]}\le-6.4\,kJ\,mol^{-1}$ (Table 1), which can be compared with the statistical values $\Delta G^{binomial}_{[Eq.\,(6)]}=-5.4\,kJ\,mol^{-1}$ calculated for the binomial distribution at 298 K.

$$(Ln^1)_3+(Ln^2)_3\rightleftharpoons(Ln^1)_2Ln^2+Ln^1(Ln^2)_2 \qquad (6)$$

A similar trend has been reported for the formation of the heterobimetallic helicates *HHH*-$[Ln^1Ln^2(L8)_3]^{6+}$, which display a monotonous increase of the deviation from the binomial distribution for the equilibrium $(Ln^1)_2+(Ln^2)_2\rightleftharpoons2Ln^1Ln^2$ with increasing difference in ionic radii $\Delta r_i=r_{Ln1}-r_{Ln2}$.[10] The deviations thus increases from $\Delta(\Delta G)=\Delta G^{exptl}_{eq}-\Delta G^{binomial}_{eq}=0\,kJ\,mol^{-1}$ for the Eu/Tb pair to $\Delta(\Delta G)=-7.4\,kJ\,mol^{-1}$ for the La/Lu pair.[10] In our case, deviations in the range $-6.5\,kJ\,mol^{-1}\le\Delta(\Delta G)=\Delta G^{exptl}_{[Eq.\,(6)]}-\Delta G^{binomial}_{[Eq.\,(6)]}\le-1.0\,kJ\,mol^{-1}$ can be calculated for the heterotrimetallic helicates (Table 1). However, we do not detect a straightforward correlation between $\Delta(\Delta G)$ and Δr_i; this reflects the increased possibilities offered by trimetallic helicates for accommodating different metal ions. We conclude that model A is oversimplified and cannot account for the subtle recognition processes occurring in heterotrimetallic complexes.

Model B—a simple statistical distribution including size-discriminating effects: Although the $\log(\beta^{Ln,exptl}_{33})$ only marginally vary along the lanthanide series for $[Ln_3(L9)_3]^{9+}$,[12] small changes may affect the statistical binomial distribution of heterotrimetallic helicates, and model B simply extends model A by considering identical absolute affinities for the terminal and central sites which can vary along the lanthanide series ($k^t_{Ln}=k^c_{Ln}=k_{Ln}$). This approach was recently successfully applied by Delangle et al. to rationalise the distribution of the heterotrimetallic sandwich complexes $[(Ln^1)_x(Ln^2)_{3-x}(L7\text{-}3H)_2(H_2O)_6]^{3+}$, in which the three metal coordination spheres are identical.[8] Equation (7) holds for the calculation of the stability constants of $[(Ln^1)_x(Ln^2)_{3-x}(L9)_3]^{9+}$, in which $\log(\beta^{Ln,exptl}_{33})$ is the experimental formation constant of the homotrimetallic helicate $[Ln_3(L9)_3]^{9+}$, and the term $\log(s)$ explicitly expresses the contribution of the increased entropy resulting from the number of different arrangements allowed in the heterotrimetallic complexes (degeneracy given in Figure 1).

$$\log(\beta^{Ln,calcd\,B}_{33}[(Ln^1)_x(Ln^2)_{3-x}])=\frac{1}{3}[x\cdot\log(\beta^{Ln^1Ln^1Ln^1,exptl}_{33})+(3-x)\cdot\log(\beta^{Ln^2Ln^2Ln^2,exptl}_{33})]+\log(s) \qquad (7)$$

The minor variations in $\log(\beta^{Ln,exptl}_{33})$ along the lanthanide series provides almost identical calculated formation constants for the homo- and heterotrimetallic species $\log(\beta^{Ln,calcd\,B}_{33})$ in agreement with the single average stability constant considered in model A (Table 2). Consequently, the distributions calculated for a ratio Ln^1:$Ln^2=1.5$:1.5 (Table S5, Supporting Information) are systematically close to the binomial distribution obtained with model A, and $\Delta G^{calcd\,B}_{[Eq.\,(6)]}$ do not deviate from the statistical binomial value ($\Delta G^{binomial}_{[Eq.\,(6)]}=-5.4\,kJ\,mol^{-1}$). This model remains inadequate for rationalising our experimental data and we deduce that specific recognition processes occur at each site that cannot be modelled by the average size-discriminating effect evidenced in the homotrimetallic helicates.

Model C—a statistical distribution including size-discriminating effects for each specific site: The application of statistical thermodynamics to the model depicted in Scheme 1 for two metal sites displaying different affinities $k^t_{Ln}\neq k^c_{Ln}$ in combination with size-discriminating effects along the lanthanide series ($k^t_{Ln^1}\neq k^t_{Ln^2}$ and $k^c_{Ln^1}\neq k^c_{Ln^2}$) leads to Equations (8)–(13) for the microscopic thermodynamic constants of each trimetallic helicate $(Ln^1)_x(Ln^2)_{3-x}$ with the simplification that $u_{Ln^1Ln^2}=u_{Ln^1Ln^1}=u_{Ln^2Ln^2}=u$. Each microscopic constant thus corresponds to the products of the absolute affinities of each occupied site, modulated by 1) the interaction parameter u for each adjacent pair in the final helicate and 2) the degeneracy factor s given in Figure 1, as similarly used for protonation reactions.[18] Note that model C reduces to model B when $k^t_{Ln^1}=k^c_{Ln^1}$ and $k^t_{Ln^2}=k^c_{Ln^2}$, and to model A when $k^t_{Ln^1}=k^c_{Ln^1}=k^c_{Ln^2}=k^c_{Ln^2}$.

$$\beta^{Ln^1Ln^1Ln^1}_{33}=(k^t_{Ln^1})^2\cdot k^c_{Ln^1}\cdot u^2 \qquad (8)$$

$$\beta_{33}^{Ln^1Ln^1Ln^2} = 2 \cdot k_{Ln^1}^t \cdot k_{Ln^1}^c \cdot k_{Ln^2}^t \cdot u^2 \quad (9)$$

$$\beta_{33}^{Ln^1Ln^2Ln^1} = (k_{Ln^1}^t)^2 \cdot k_{Ln^2}^c \cdot u^2 \quad (10)$$

$$\beta_{33}^{Ln^1Ln^2Ln^2} = 2 \cdot k_{Ln^1}^t \cdot k_{Ln^2}^c \cdot k_{Ln^2}^t \cdot u^2 \quad (11)$$

$$\beta_{33}^{Ln^2Ln^1Ln^2} = (k_{Ln^2}^t)^2 \cdot k_{Ln^1}^c \cdot u^2 \quad (12)$$

$$\beta_{33}^{Ln^2Ln^2Ln^2} = (k_{Ln^2}^t)^2 \cdot k_{Ln^2}^c \cdot u^2 \quad (13)$$

Only five of these equations are mathematically independent, and we can thus theoretically extract the four parameters $k_{Ln^1}^t$, $k_{Ln^2}^t$, $k_{Ln^1}^c$ and $k_{Ln^2}^c$ for a given Ln^1/Ln^2 pair for which all four heterotrimetallic species are observed in solution and their formation constants estimated by ^{1}H NMR spectroscopy [u cannot be obtained as an independent parameter, since Eqs. (8)–(13) are all multiplied by the same factor u^2]. However, such a statistical description requires an over-determined system for extracting physically meaningful parameters,[18] and for most Ln^1/Ln^2 pairs, only a partial set of formation constants is at hand for the heterotrimetallic helicates (Table 2). To maximise the ratio between experimental data and fitted parameters, we simplified the model by 1) neglecting the interaction between two adjacent lanthanides ($\Delta E = 0$ and $u = 1$) and 2) incorporating in the fitting process the formation constants $\beta_{23}^{Ln,exptl}$ of the unsaturated complexes $[Ln_2(L9)_3]^{6+}$ determined by spectrophotometric titration[12] [Eqs. (14) and (15) take into account the two possible arrangements in which the metal ions occupy either the two terminal sites or the central site and one terminal site in $[Ln_2(L9)_3]^{6+}$].[18] Under these conditions and depending on the specific Ln^1/Ln^2 pair, we have considered 5–7 independent experimental stability constants (and their associated equations) for extracting the four parameters $k_{Ln^1}^t$, $k_{Ln^2}^t$, $k_{Ln^1}^c$ and $k_{Ln^2}^c$ by using nonlinear least-squares techniques (Table 4).[19] Good agreement is obtained for similar parameters extracted from the analyses of different pairs, which supports the reliability of the fitting process.

$$\beta_{23}^{Ln^1Ln^1} = (k_{Ln^1}^t)^2 + 2 \cdot k_{Ln^1}^t \cdot k_{Ln^1}^c \cdot u \quad (14)$$

$$\beta_{23}^{Ln^2Ln^2} = (k_{Ln^2}^t)^2 + 2 \cdot k_{Ln^2}^t \cdot k_{Ln^2}^c \cdot u \quad (15)$$

The formation constants $\log(\beta_{33}^{Ln^iLn^kLn^l,calcd\,C})$ calculated with k_{Ln}^t and k_{Ln}^c listed in Table 4 and Equations (8)–(13) are in good agreement with the accessible experimental data obtained by spectrophotometry and ^{1}H NMR spectroscopy (Table 2). Moreover, the heterotrimetallic complexes that are not detected by NMR spectroscopy (and for which no experimental formation constant is available) systematically display calculated $\beta_{33}^{Ln^iLn^kLn^l,calcd\,C}$ which are approximately one order of magnitude smaller than the related constants for the complexes $(Ln^1)_x(Ln^2)_{3-x}$ observed by ^{1}H NMR spectroscopy. The distributions calculated for a ratio $Ln^1:Ln^2 = 1.5:1.5$ and $[L9]_{tot} = 10^{-2}$ M (Table 5) show a satisfying correlation with the experimental data according to the limited sophistication of model C (Figure 5). Consequently, the $\Delta G_{[Eq.\,(6)]}^{calcd\,C}$ values calculated for each Ln^1/Ln^2 pair with this model ($-11.0\,kJ\,mol^{-1} \le \Delta G_{[Eq.\,(6)]}^{exptl} \le -6.4\,kJ\,mol^{-1}$, Table 5)

Table 4. Absolute affinities for the terminal ($\log(k_{Ln}^t)$) and central ($\log(k_{Ln}^c)$) metal sites in the triple-stranded helicates $[Ln_3(L9)_3]^{9+}$, obtained with model C.

Ln	r_{Ln} [Å][a]	$\log(k_{Ln}^t)$	$\log(k_{Ln}^c)$
La	1.216	12.50(5)	9.59(8)
Nd	1.163	12.83(5)	9.18(8)
Sm	1.132	12.93(5)	9.09(8)
Eu	1.120	12.98(5)	8.94(8)
Y	1.075	13.01(5)	8.61(8)
Yb	1.042	12.97(5)	8.51(8)
Lu	1.032	12.88(5)	8.44(8)

[a] r_{Ln} = nine-coordinate ionic radii taken from reference [22].

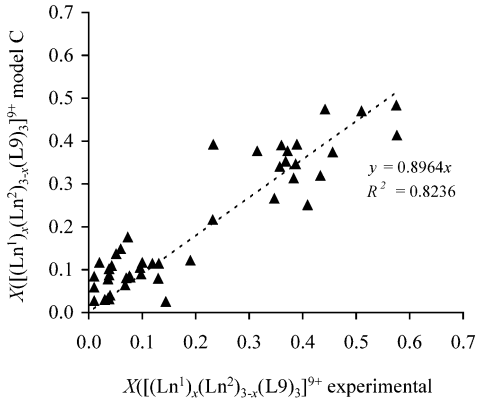

Figure 5. Plots of the experimental mole fractions of $[(Ln^1)_x(Ln^2)_{3-x}(L9)_3]^{9+}$ determined by ^{1}H NMR spectroscopy as a function of the corresponding mole fraction calculated with model C. The dotted line estimates the quality of this correlation.

Table 5. Mole fractions of homo- and heterotrimetallic helicates $[(Ln^1)_x(Ln^2)_{3-x}(L9)_3]^{9+}$ ($x = 0$, 1, 2, 3) calculated with model C for $Ln^1:Ln^2:L9 = 1.5:1.5:3.0$ ($[L9]_{tot} = 10^{-2}$ M, 298 K).

Ln^1	Ln^2	Δr_i [Å][a]	$[Ln_3^1L_3]^{9+}$	$[Ln^1Ln^2Ln^1L_3]^{9+}$	$[Ln^1Ln^1Ln^2L_3]^{9+}$	$[Ln^2Ln^1Ln^2L_3]^{9+}$	$[Ln^1Ln^2Ln^2L_3]^{9+}$	$[Ln_3^2L_3]^{9+}$	$\Delta G_{[Eq.\,(6)]}^{calcd\,C}$ [kJ mol^{-1}]
La	Lu	0.184	0.08	0.01	0.39	0.47	0.03	0.03	−10.7
La	Yb	0.174	0.08	0.01	0.39	0.48	0.03	0.03	−11.0
La	Y	0.141	0.08	0.01	0.39	0.47	0.03	0.04	−10.4
Nd	Lu	0.131	0.12	0.03	0.38	0.31	0.10	0.08	−7.0
Sm	Lu	0.100	0.11	0.05	0.34	0.25	0.15	0.11	−6.3
La	Eu	0.096	0.09	0.01	0.38	0.41	0.06	0.06	−8.7
Eu	Lu	0.088	0.12	0.07	0.32	0.22	0.18	0.12	−5.9
La	Sm	0.084	0.08	0.02	0.35	0.37	0.08	0.09	−7.8
Sm	Y	0.057	0.11	0.04	0.35	0.27	0.14	0.10	−6.4
Y	Lu	0.043	0.13	0.12	0.26	0.13	0.24	0.12	−5.4

[a] $\Delta r_i = r_{Ln1} - r_{Ln2}$ for nine-coordinate ionic radii taken from reference [22].

closely match the experimental values for each pair ($-11.9\ \mathrm{kJ\,mol^{-1}} \le \Delta G^{\mathrm{calcd\,C}}_{[\mathrm{Eq.\,(6)}]} \le -6.4\ \mathrm{kJ\,mol^{-1}}$, Table 1).

The variation of $\log(k^{c}_{\mathrm{Ln}})$ along the lanthanide series displays an inverted electrostatic trend[7a] leading to a decreased affinity of the central site for smaller lanthanides (Figure 6a). This behaviour is reminiscent of the corresponding abrupt decrease in formation constants reported for the monometallic model of the central N_9 site $[Ln(L10)_3]^{3+}$, which is attributed to intramolecular interstrand stacking interactions preventing the contraction of the cavity required for accommodating heavy Ln^{III} ions.[20] A parallel effect occurs in $[Ln_3(L9)_3]^{9+}$; this explains the reluctance of the smaller Ln^2 to occupy the central site and the associated negligible quantities of $Ln^1Ln^2Ln^1$ and $Ln^1Ln^2Ln^2$ helicates detected by ^{1}H NMR spectroscopy (Table 1). On the other hand, $\log(k^{t}_{\mathrm{Ln}})$ displays a concave dependence along the lanthanide series with a maximum affinity around Ln = Y (Figure 6b; the ionic radius of Y^{III} is similar to that of Ho^{III}).[22] This trend has no precedent in the monometallic model of the facial N_6O_3 site in $[Ln(L11)]^{3+}$, which displays a weak standard electrostatic trend.[21] We tentatively attribute the specific bowl-shaped dependence of $\log(k^{t}_{\mathrm{Ln}})$ to structural constraints induced by the adjacent central site in the wrapping process of the strands (i.e., mechanical coupling). However, possible variations of the intermetallic interactions for each specific Ln^1/Ln^2 cannot be ruled out, and a definitive interpretation requires the extraction of explicit $u_{\mathrm{Ln^1Ln^2}}$ parameters.

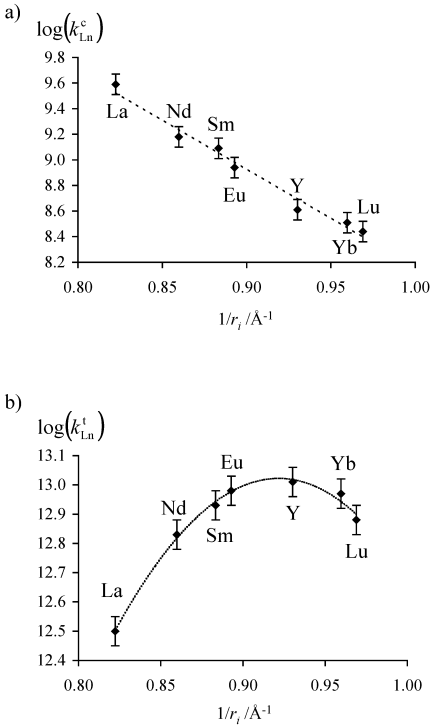

Figure 6. Absolute affinities for a) the central site ($\log(k^{c}_{\mathrm{Ln}})$) and b) the terminal sites ($\log(k^{t}_{\mathrm{Ln}})$) in the triple-stranded trimetallic helicates $[Ln_3(L9)_3]^{9+}$ as a function of the reciprocal nine-coordinate ionic radii. The trend lines are only guides for the eye.

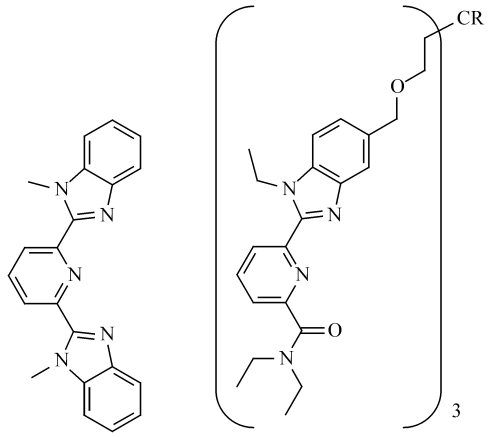

L10 **L11**

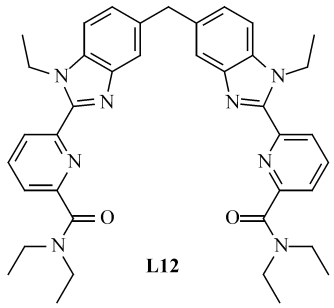

L12

Since $\Delta G^{\mathrm{calcd\,C}}_{[\mathrm{Eq.\,(6)}]}$ for the global equation are complicated functions of k^{c}_{Ln} and k^{t}_{Ln} [Eq. (16), whereby $\beta^{\mathrm{Ln}^i\mathrm{Ln}^k\mathrm{Ln}^l}_{33}$ are given by Eqs. (8)–(13)], their non-monotonous and different dependences on $\Delta r_i = r_{\mathrm{Ln1}} - r_{\mathrm{Ln2}}$ (Figure 6) prevent any straightforward correlations between $\Delta G_{[\mathrm{Eq.\,(6)}]}$ and Δr_i, in contrast to the monotonous decrease of this parameter with increasing Δr_i previously observed for the analogous bimetallic complexes *HHH*-$[(Ln)_2(L8)_3]^{6+}$.[10]

$$\Delta G^{\mathrm{calcd\,C}}_{[\mathrm{Eq.\,(6)}]} = -RT\{\ln(\beta^{\mathrm{Ln^1Ln^1Ln^2}}_{33} + \beta^{\mathrm{Ln^1Ln^2Ln^1}}_{33}) + \ln(\beta^{\mathrm{Ln^1Ln^2Ln^2}}_{33} + \beta^{\mathrm{Ln^2Ln^1Ln^2}}_{33}) - \ln(\beta^{\mathrm{Ln^1Ln^1Ln^1}}_{33}) - \ln(\beta^{\mathrm{Ln^2Ln^2Ln^2}}_{33})\} \quad (16)$$

Interestingly, we can rationally predict the speciation for any Ln^1/Ln^2 pairs for which individual k^{c}_{Ln} and k^{t}_{Ln} values are reported in Table 4. Application of Equations (8)–(13) for the Y/Lu pair provides calculated formation constants $\log(\beta^{\mathrm{Ln}^i\mathrm{Ln}^k\mathrm{Ln}^l,\mathrm{calcd\,C}}_{33})$ for the $(Y)_x(Lu)_{3-x}$ ($x = 0$–3) complexes with very similar magnitudes ($34.2 \le \log(\beta^{\mathrm{Ln}^i\mathrm{Ln}^k\mathrm{Ln}^l,\mathrm{calcd\,C}}_{33}) \le 34.8$, Table 2), which translates into a speciation very close to the binomial distribution (Table S5, Supporting Information). The concomitant existence in acetonitrile of six structurally related diamagnetic complexes in comparable concentrations explains the very complicated ^{1}H NMR spectra observed for the Y/Lu pair, which escape detailed analysis. This peculiar situation results from the similar preferences of both Ln^1 = Y and Ln^2 = Lu for the terminal site and their reluctance to enter the central site (Table 4, Figure 6).

Characterisation and isolation of a specific heterotrimetallic complex—EuLaEu: We now explore distortions from the

thermodynamic speciation that can occur during the crystallisation (i.e., isolation) process. We selected the La/Eu pair, because its specific k^{c}_{Ln} and k^{t}_{Ln} favour formation of the heterotrimetallic EuLaEu species. For a stoichiometric ratio La:Eu = 1:2 and $[L9]_{tot} = 10^{-2}$ M in acetonitrile, we calculate that EuLaEu (48%), Eu_3 (23%) and LaLaEu (19%) are the major components of the mixture, while LaEuEu (8%) and La_3 + LaEuLa (2%) can be neglected, in agreement with ^{1}H NMR data (Table S3, Supporting information). Slow diffusion of *tert*-butyl methyl ether into this mixture produces only amorphous powders, but the replacement of acetonitrile with nitromethane, a solvent with similar dielectric and complexation characteristics (the experimental distribution found in CD_3NO_2 by ^{1}H NMR spectroscopy is similar within experimental error to that found in CD_3CN) provides X-ray-quality prisms of $[La_{0.96}Eu_{2.04}(L9)_3](CF_3SO_3)_9(CH_3NO_2)_9$ (**1**). The crystal structure of **1** consists of discrete $[EuLaEu(L9)_3]^{9+}$ ions, uncoordinated triflate anions and solvent molecules. The anions and solvent molecules are partially disordered, but show no other features of interest. In contrast to $[Eu_3(L9)_3](CF_3SO_3)_9(CH_3CN)_9(H_2O)_2$, which crystallises in the triclinic crystal system, space group $P\bar{1}$ ($Z = 2$),[12] the analogous heterotrimetallic complex **1** crystallises in the monoclinic crystal system, space group $P2_1/c$, and these complexes are thus not isostructural. However, the molecular structures of the two ions $[EuLaEu(L9)_3]^{9+}$ and $[Eu_3(L9)_3]^{9+}$ are very similar, except for two significant differences (Figure 7, Table 6). First, the less distorted overall shape of the triple helix for EuLaEu implies 1) reduced bending (Eu···La···Eu 177.97(4)° vs Eu···Eu···Eu 173.71(1)° in Eu_3)[12] and 2) more regular positioning of the metal ions along the helical axis (Eu1···La1 9.105(1) and La1···Eu2 9.126(1) Å vs Eu2···Eu1 9.3165(7) and Eu1···Eu3 9.0762(7) Å).[12] Second, the coordination sphere of the central site primarily occupied by La1 is significantly expanded, with average La–N(benzimidazole) (2.66(2) Å) and La–N(pyridine) (2.66(1) Å) bond lengths that are significantly longer than those reported for the central Eu1 in $[Eu_3(L9)_3]^{9+}$ (2.59(1) and 2.58(2) Å, respectively).[12] This expansion of the cavity fairly matches that expected for the replacement of nine-coordinate Eu^{III} ($r^{CN=9}_{Eu} = 1.120$ Å)[22] in Eu_3 with La^{III} ($r^{CN=9}_{La} = 1.216$ Å)[22] and confirms the location of a lanthanum atom in the central site of EuLaEu. In this context, the almost identical bond lengths and coordination spheres observed for the terminal sites in both trimetallic helicates justify the systematic location of Eu^{III} in the terminal sites.

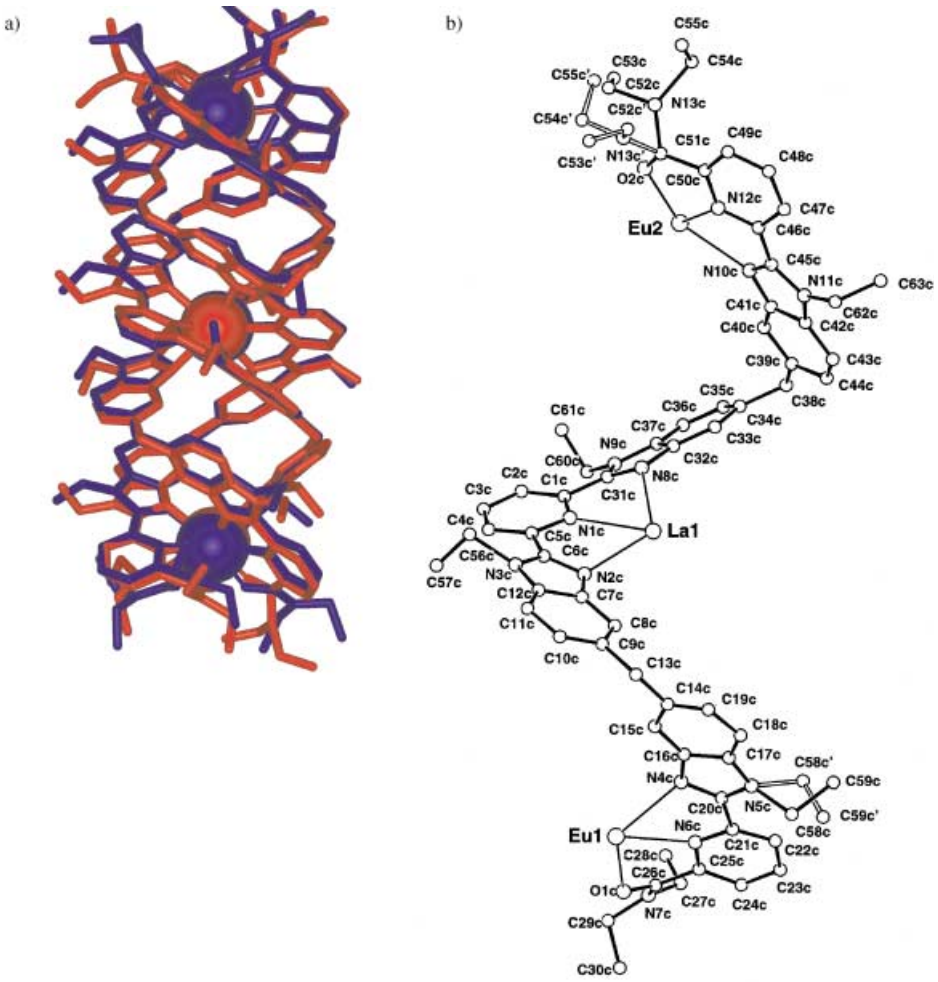

Figure 7. a) Optimised superimposition of the molecular structures of $[EuLaEu(L9)_3]^{9+}$ (blue) and $[Eu_3(L9)_3]^{9+}$ (red) viewed perpendicular to the pseudo-C_3 axis. b) Perspective view of one strand showing the atomic numbering scheme and the disorders affecting strand c.

A thorough scrutiny of the helical wrapping of the strands, based on the calculation of pitches P_{ij} for the nine successive helical portions F1–F9 (as previously described for $[Eu_3(L9)_3]^{9+}$, Table S6, Supporting Information),[12] shows only minor structural changes in the global shape when Eu^{III} occupying the central site in $[Eu_3(L9)_3]^{9+}$ is replaced with La^{III} in $[EuLaEu(L9)_3]^{9+}$. This indicates that the crystals of **1** may indeed contain mixtures of the very similar complexes LaLaEu, EuLaEu and Eu_3, which correspond to 90% of the speciation in solution before crystallisation. Each metal site in **1** was thus refined with adjustable population parameters (PP) characterising the dual introduction of Eu^{III} or La^{III}. Convergence occurs when the two terminal sites are occupied by about 90% Eu^{III} and 10% La^{III} ($PP_{Eu1} = 0.88(3)$, $PP_{La11} = 0.12(3)$ and $PP_{Eu2} = 0.90(3)$, $PP_{La22} = 0.10(3)$), while the central site contains 74(3)% of La^{III} and 26(3)% of Eu^{III},

Table 6. Selected distances [Å] and angles [°] for $[La_{0.96}Eu_{2.04}(L9)_3](CF_3SO_3)_9(CH_3NO_2)_9$ (**1**) and $[Eu_3(L9)_3](CF_3SO_3)_9(CH_3CN)_9(H_2O)_2$.[12]

	$[EuLaEu(L9)_3]^{3+}$				$[Eu_3(L9)_3]^{3+}$[12]		
intermetallic distances							
Eu1···La1	9.105(1)			Eu1···Eu2	9.3165(7)		
Eu2···La1	9.126(1)			Eu1···Eu3	9.0762(7)		
Eu1···Eu2	18.228(1)			Eu2···Eu3	18.3650(9)		
bond lengths	ligand a	ligand b	ligand c		ligand a	ligand b	ligand c
La1–N1	2.64(1)	2.69(1)	2.64(1)	Eu1–N1	2.61(1)	2.56(1)	2.61(1)
La1–N2	2.69(1)	2.67(1)	2.62(1)	Eu1–N2	2.53(1)	2.59(1)	2.60(1)
La1–N8	2.65(1)	2.66(1)	2.67(1)	Eu1–N8	2.60(1)	2.58(1)	2.59(1)
Eu1–O1	2.37(1)	2.37(1)	2.46(1)	Eu2–O1	2.38(1)	2.38(1)	2.41(1)
Eu1–N4	2.53(1)	2.58(1)	2.67(1)	Eu2–N4	2.60(1)	2.55(1)	2.64(1)
Eu1–N6	2.60(1)	2.65(1)	2.57(1)	Eu2–N6	2.59(1)	2.65(1)	2.65(1)
Eu2–O2	2.46(1)	2.41(1)	2.37(1)	Eu3–O2	2.38(1)	2.40(1)	2.41(1)
Eu2–N10	2.61(1)	2.61(1)	2.54(1)	Eu3–N10	2.57(1)	2.67(1)	2.59(1)
Eu2–N12	2.57(1)	2.60(1)	2.62(1)	Eu3–N12	2.60(1)	2.57(1)	2.57(1)
angles							
Eu1···La1···Eu2	177.97(4)			Eu2···Eu1···Eu3	173.71(1)		

thus leading to the global formula $[La_{0.96}Eu_{2.04}(L9)_3]^{9+}$. Although the *R* factor and goodness of fit are slightly improved relative to the original refinement considering $[EuLaEu(L9)_3]^{9+}$ as a pure complex, the structural parameters (bond lengths, bond angles and torsion angles) are identical within statistical uncertainties for both refinements, and the data reported in this contribution correspond to those obtained for $[La_{0.96}Eu_{2.04}(L9)_3](CF_3SO_3)_9(CH_3NO_2)_9$ (**1**). This result strongly suggests that the crystal structure indeed reflects the crystallisation of $[EuLaEu(L9)_3]^{9+}$ as the major component with co-crystallisation of non-negligible quantities of $[LaLaEu(L9)_3]^{9+}$ and $[Eu_3(L9)_3]^{9+}$. Elemental analyses of the metal content by ICP-MS after mineralisation of crystals of **1** gave a Eu:La ratio of 2.23(3):1, which translates into the formula $[La_{0.93}Eu_{2.07}(L9)_3]^{9+}$, in fair agreement with X-ray analysis. Finally, we used high-resolution emission spectroscopy to establish the specific occupancy of the different sites with luminescent Eu^{III} in crystals of **1**. A previous detailed photophysical investigation of pure $[Eu_3(L9)_3](CF_3SO_3)_9$ ascribed the Eu-centred $^5D_0 \rightarrow {}^7F_0$ transition originating from the two equivalent terminal EuN_6O_3 sites to band **t** (17219 cm^{-1} at 5 K), and that from the central EuN_9 site to band **c** (17238 cm^{-1} at 5 K).[12] Since the intrinsic concentration of the terminal sites in $[Eu_3(L9)_3]^{9+}$ is twice that of the central site and the quantum yield associated with the central EuN_9 chromophore is smaller than that of EuN_6O_3,[12] the intensity of the emission originating from the central site F_c is significantly weaker than that from the terminal sites F_t (Figure 8). Gaussian decomposition of the two $^5D_0 \rightarrow {}^7F_0$ transitions observed in the emission spectrum of $[Eu_3(L9)_3]^{9+}$ obtained on broadband excitation of the $Eu(^5D_2)$ level at 15 K ($\tilde{\nu}_{exc} = 21468\ cm^{-1}$, Figure 8a) leads to $F_c/(F_c + F_t) = 0.27$, which can be used with Equation (17) for calibrating the ratio of the emission efficiency factor ρ associated with each site: $\rho_c/\rho_t = 0.74$.

$$\frac{F_c}{F_c + F_t} = \frac{\rho_c}{\rho_c + 2\rho_t} = 0.27 \qquad (17)$$

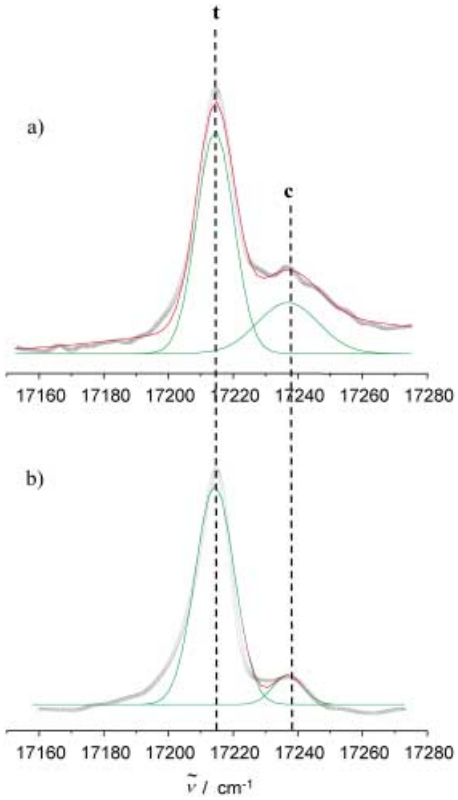

Figure 8. Gaussian decomposition of the $Eu(^5D_0 \rightarrow {}^7F_0)$ transitions originating from the terminal (band **t**) and central (band **c**) metal sites in the emission spectra of a) $[Eu_3(L9)_3]^{9+}$ and b) $[EuLaEu(L9)_3]^{9+}$ ($\tilde{\nu}_{exc} = 21468\ cm^{-1}$, 15 K).

The emission spectrum of the heterotrimetallic helicate **1** (Figure 8b) is similar to that recorded for $[Eu_3(L9)_3](CF_3SO_3)_9$ (Figure 8a), except for the much smaller ratio $F_c/(F_c + F_t) = 0.094$. The observation of a faint residual emission from the central site at 17238 cm^{-1} confirms the partial replacement of non-emissive La^{III} by luminescent Eu^{III}, in agreement with X-ray analysis. According to the

original speciation of complexes in solution before crystallisation, EuLaEu (48%) and Eu_3 (23%) are the two major components in the mixture, and co-crystallisation may qualitatively explain the observation of some Eu^{III} occupying the central site. Equation (18) holds for a binary mixture of $(1-\alpha)$(EuLaEu) + α(Eu_3) in the solid state, and $\alpha = 0.28$ can be calculated, since $\rho_c/\rho_t = 0.74$. This finally translates into a global stoichiometry $[La_{(1-\alpha)}Eu_{(2+\alpha)}(L9)_3]^{9+} = [La_{0.72}Eu_{2.28}(L9)_3]^{9+}$, which does not agree with the elemental analysis.

$$\frac{F_c}{F_c + F_t} = \frac{\alpha\rho_c}{\alpha\rho_c + 2\rho_t} = 0.094 \quad (18)$$

We deduce that the third significant component LaLaEu of the original solution (19%) is also incorporated in the final crystals; this consequently introduces some non-emissive La^{III} in the terminal sites. Taking the average population parameter of the lanthanum atom found by X-ray analysis in the terminal sites ($PP_{La(terminal)} \approx 0.1$), we calculate that LaLaEu contributes 20% in the solid-state mixture, while $(1-\alpha)$(EuLaEu) + α(Eu_3) accounts for the remaining 80%. Equation (19) thus holds, and we obtain $\alpha = 0.32$ with $\rho_c/\rho_t = 0.74$.

$$\frac{F_c}{F_c + F_t} = \frac{0.8\,\alpha \cdot \rho_c}{0.8\,\alpha \cdot \rho_c + 1.8\rho_t} = 0.094 \quad (19)$$

This translates into $PP_{Eu(central)} = 0.8\alpha = 0.26$ and a global composition $[La_{(1.2-0.8\alpha)}Eu_{(1.8+0.8\alpha)}(L9)_3]^{9+} = [La_{0.94}Eu_{2.06}(L9)_3]^{9+}$, which agrees with both elemental analysis and X-ray diffraction data. The combination of the three techniques (X-ray diffraction, elemental analysis, high-resolution emission spectroscopy) eventually demonstrates that in the crystal of **1** $[EuLaEu(L9)_3]^{9+}$ (54%) is co-crystallised with $[LaLaEu(L9)_3]^{9+}$ (20%) and $[Eu_3(L9)_3]^{9+}$ (26%); this closely reflects the calculated speciation in the original liquor (48, 19, 23%). We conclude that no significant enrichment occurs during the crystallisation process of the triple-helical complexes $[(La)_x(Eu)_{3-x}(L9)_3]^{9+}$, which display sufficiently similar characteristics for their statistical incorporation into the crystal lattice.

Conclusion

Our investigation of the formation of the homo- and heterotrimetallic helicates $[(Ln^1)_x(Ln^2)_{3-x}(L9)_3]^{9+}$ ($x = 0$–3) demonstrates that the classical statistical thermodynamic models A and B, which consider identical affinities for the terminal and central sites, fail to rationalise the speciation in solution and the associated thermodynamic formation constants. The assignment of different absolute affinities to the terminal (k^t_{Ln}) and the central (k^c_{Ln}) sites is evidently a consequence of the respective coordination spheres N_6O_3 and N_9 provided by the wrapped strands in $[Ln_3(L9)_3]^{9+}$, but their estimation strongly depends on the sophistication of the statistical thermodynamic model. Our preliminary set of data collected for seven different ions along the lanthanide series (La, Nd, Sm, Eu, Yb, Lu, Y), of which the heterotrimetallic complexes of only ten pairs have been explored, leads us to neglect the interaction parameter $u_{Ln^1Ln^2} = \exp(-\Delta E_{Ln^1Ln^2}/RT) = 1$ (model C), and the resulting k^t_{Ln} and k^c_{Ln} display intriguing, but continuous, dependence on the lanthanide size along the series. As expected from previous studies on the monometallic triple-helical model $[Ln(L10)_3]^{3+}$,[20] the central nine-coordinate N_9 site in $[Ln_3(L9)_3]^{9+}$ favours complexation of large Ln^{III} ions and thus leads to a reverse electrostatic trend (Figure 6a). However, the peak of selectivity around Ln = Ho (Figure 6b) observed for the terminal site has no precedent in the monometallic model $[Ln(L11)]^{3+}$,[21] and its definitive interpretation should await until sufficient non-correlated thermodynamic data are available for extracting reliable interaction parameters $u_{Ln^1Ln^2}$. Although a satisfying fit of the available micro- and macroscopic thermodynamic formation constants for $[(Ln^1)_x(Ln^2)_{3-x}(L9)_3]^{9+}$ was obtained with the rough sets of k^c_{Ln} and k^t_{Ln} (collected in Table 4), explicit values for the interaction parameters $u_{Ln^1Ln^2}$ remain crucial for rationalising fine recognition processes resulting from intermetallic electronic, electrostatic or mechanical coupling. Preliminary attempts to extract a mean parameter $u_{Ln^1Ln^2} = u_{Ln^1Ln^1} = u_{Ln^2Ln^2} = u \neq 1$, together with the absolute affinities for some favourable Ln^1/Ln^2 pairs [i.e., pairs for which seven independent stability constants are available, Eqs. (8)–(15)] show drastic correlations between the fitted parameters and no significant improvement of the quality of the thermodynamic model. A more sophisticated description thus requires simultaneous consideration of the formation constants for the analogous monometallic $[Ln(L12)_3]^{3+}$ (β^{Ln}_{13}) and bimetallic helicates $[(Ln^1)_x(Ln^2)_{2-x}(L12)_3]^{6+}$ ($x = 0, 1, 2$; $\beta^{Ln^1Ln^2}_{23}$),[15] because β^{Ln}_{13} and $\beta^{Ln^1Ln^2}_{23}$ depend only on k^t_{Ln} and $u_{Ln^1Ln^2}$ The combination of mono-, bi- and trimetallic thermodynamic data should give sets of 12 independent equations for each Ln^1/Ln^2 pair from which at least five parameters (including $u_{Ln^1Ln^2}$) could be reasonably extracted, and research along this line is in progress. Interestingly, model C can be easily extended and adapted for numerous types of supramolecular polymetallic assemblies obtained under thermodynamic equilibria, thus opening perspectives for the rational programming and preparation of heterometallic complexes exhibiting novel functions resulting from specific intermetallic communications.[13,23] In this context, the predicted and observed isolation of about 50% of $[EuLaEu(L9)_3]^{9+}$ from a well-defined mixture highlights the potential and limitation of this approach, because the different heterotrimetallic helicates are too similar to allow selective crystallisation of one particular complex. In other words, the preparation of heterometallic triple-stranded helicates depends on our capacity 1) to combine different sites along the strands displaying specific affinities for Ln^{III} and 2) to rationalise intermetallic couplings which are responsible for further ultrafine tuning and selectivity.

Experimental Section

Solvents and starting materials were purchased from Fluka AG (Buchs, Switzerland) and used without further purification unless otherwise

stated. Acetonitrile was distilled from CaH_2. The ligand 2,6-bis{1-ethyl-5-{1-ethyl-2-[6-(*N*,*N*-diethylcarbamoyl)pyridin-2-yl]benzimidazol-5-methylene}benzimidazole-2-yl}pyridine (L9) was prepared according to a literature procedure.[12] The triflate salts $Ln(CF_3SO_3)_3{\cdot}xH_2O$ (Ln = La–Lu) were prepared from the corresponding oxides (Rhodia, 99.99%). The Ln content of solid salts was determined by complexometric titrations with Titriplex III (Merck) in the presence of urotropine and xylene orange.[24]

Preparation of the complexes $[(Ln^1)_x(Ln^2)_{3-x}(L9)_3]^{9+}$ (Ln^1, Ln^2 = La, Nd, Sm, Eu, Yb, Lu, Y; x = 0, 1, 2, 3). L9 (7.25 mg, 7×10^{-6} mol), $Ln^1(CF_3SO_3)_3{\cdot}xH_2O$ and $Ln^2(CF_3SO_3)_3{\cdot}xH_2O$ in variable proportions (condition: $[Ln^1]+[Ln^2]=[Ln_{tot}]=7\times10^{-6}$ mol) were mixed in dichloromethane/acetonitrile (1/1, 2 mL). After stirring for 3 h at room temperature, the solution was evaporated, dried under vacuum and the solid residue dissolved in CD_3CN (700 μL). The resulting solution was equilibrated for 48 h at 298 K prior to ^{1}H NMR measurement. For ESI-MS spectra, the final solutions were diluted with acetonitrile (13.3 mL) to give $[L9]_{tot}=5\times10^{-4}$ M.

Crystal structure determination of $[La_{0.96}Eu_{2.04}(L9)_3](CF_3SO_3)_9(CH_3NO_2)_9$ (1): Slow diffusion of *tert*-butyl methyl ether into a mixture of $La(CF_3SO_3)_3$:$Eu(CF_3SO_3)_3$:L9 = 1:2:3 ($[L9]_{tot}=10^{-2}$ M) in nitromethane provided X-ray-quality prisms of $[La_{0.96}Eu_{2.04}(L9)_3](CF_3SO_3)_9(CH_3NO_2)_9$ (**1**). $Eu_{2.04}La_{0.96}C_{207}H_{222}N_{48}O_{51}F_{27}S_9$; $M_r=5443.7$; $\mu=0.81$ mm^{-1}, $\rho_{exptl}=1.397$ g cm^{-3}, monoclinic, $P2_1/c$, $Z=4$, $a=21.8000(14)$, $b=33.5750(13)$, $c=35.5235(18)$ Å, $\beta=95.339(7)°$, $V=25888(2)$ Å^3; transparent prism, 0.052 × 0.17 × 0.46 mm, mounted on a quartz fiber with protective oil. Cell dimensions and intensities were measured at 200 K on a Stoe IPDS diffractometer with graphite-monochromated $Mo_{K\alpha}$ radiation ($\lambda=0.7107$ Å); 119897 measured reflections, $2\theta_{max}=44.7°$, 32909 unique reflections of which 14460 were observable [$|F_o|>4\sigma(F_o)$]; $R_{int}=0.095$ for 85737 equivalent reflections. Data were corrected for Lorentzian and polarisation effects and for absorption (min/max transmission = 0.8180/0.9579). The structure was solved by direct methods (SIR97),[25] and all other calculations were performed with the XTAL[26] and ORTEP[27] programs. Full-matrix least-squares refinement based on F using weights of $1/[\sigma^2(F_o)+0.00015(F_o^2)]$ gave final $R=0.061$, $wR=0.063$ and $S=1.52(1)$ for 2956 variables and 15775 contributing reflections. The final difference electron density map showed a maximum of +1.70 and a minimum of −1.27 e Å^{-3}. The hydrogen atoms were placed in calculated positions and contributed to F_c calculations. The population parameters of the metal sites Eu1, La1 and Eu2 (major) were refined (Eu1, La1, Eu2 = 0.88(3), 0.74(3), 0.90(3)), and those of the respective La11, Eu11, La22 (minor) were constrained to be complementary to unity. No restriction was applied between the population parameters of the terminal Eu1 and Eu2 atomic sites. The anisotropic displacement parameters of the minor sites were constrained to be identical to those of the major sites. The methyl C61b, ethyl C58c-C59c and diethylamide N13c-C52c-C53c-C54c-C55c groups (14 atoms) were disordered, and each group was refined on two distinct positions with PP = 0.5 and isotropic displacement parameters. The anions were refined with anisotropic displacement parameters, except for the nine carbon atoms, and restraints on bond lengths and angles. The solvent molecules were located on 14 sites (4 sites with PP = 1 and 10 sites with PP = 0.5) and refined with isotropic displacement parameters and restraints on bond lengths and angles. On account of the ambiguity in the location of the methyl groups, the hydrogen atoms of the nitromethane solvent molecules were not calculated. CCDC 218566 (**1**) contains the supplementary crystallographic data for this paper. These data can be obtained free of charge via www.ccdc.cam.ac.uk/conts/retrieving.html (or from the Cambridge Crystallographic Data Centre, 12 Union Road, Cambridge CB2 1EZ, UK; fax: (+44) 1223-336-033; or deposit@ccdc.cam.uk).

Spectroscopic and analytical measurements: IR spectra were obtained from KBr pellets with a Perkin–Elmer 883 spectrometer. ^{1}H NMR spectra were recorded on a Broadband Varian Gemini 300 and on a Brucker DRX-500 spectrometer at 298 K. Chemical shifts are given in ppm versus TMS. The relative proportion of each complex was determined by integration of the ^{1}H NMR signals at different Ln^1:Ln^2:L9 ratios. The associated stability constants were estimated from distributions simulated with the program MINEQL$^+$.[15] ESI-MS spectra were recorded from 5×10^{-4} M acetonitrile solutions with plastic microchips (DiagnoSwiss, Monthey, Switzerland) used as single-use infusion devices[28] on a triple-quadrupole linear ion trap mass spectrometer (QqLIT)[29] (Q TRAP, AB/MDS Sciex, Concord, Canada). Microchips were cut into a V shape at one end of the channel (120 μm in width, 45 μm in height and 1 cm in length), and a polypropylene reservoir was placed on the other end. The open-ended tip was positioned and centred with a home-made source 2 mm in front of the MS front plate. A voltage of 3.5 to 3.8 kV was applied to 50 μL of sample in the reservoir with a platinum electrode (front plate: 1 kV). Mass spectra were acquired either as full-scan Q1 (unit mass resolution) averaged over typically 30 s, or as enhanced-resolution (ER) spectra centred on the mass of interest by using the linear ion trap with a trap fill time of 5 ms and a LIT scan rate of 250 Th s^{-1} averaged over 30 s. The experimental procedures for high-resolution, laser-excited luminescence measurements have been published previously.[30] Solid-state samples were finely powdered, and low temperature (295–5 K) was achieved by means of a Cryodyne Model 22 closed-cycle refrigerator from CTI Cryogenics. Luminescence spectra were corrected for the instrumental function, but not excitation spectra. The metal contents of the complex were determined by ICP-MS (HP 4500 ICP MS) after oxidative mineralisation of the sample (standard solutions: Eu and La 1.0 mg mL^{-1} in 2% aqueous nitric acid (Acros)).

Acknowledgement

We are grateful to Mr Frédéric Gumy and Dr Michel Martin for their technical assistance. This work is supported through grants from the Swiss National Science Foundation.

[1] a) Y. Shen, T. Riedener, K. L. Bray, *Phys. Rev. B* **2000**, *61*, 11460; b) D. R. Gamelin, H. U. Güdel, *Acc. Chem. Res.* **2000**, *33*, 235; c) R. T. Wegh, H. Donker, K. D. Oskam, A. Meijerink, *J. Lumin.* **1999**, *82*, 93; d) C. Ronda, *J. Lumin.* **2002**, *100*, 301.

[2] a) O. Kahn, *Adv. Inorg. Chem.* **1995**, *43*, 179; b) O. Kahn, *Acc. Chem. Res.* **2000**, *33*, 647; c) M. Sakamoto, K. Manseki, H. Okawa, *Coord. Chem. Rev.* **2001**, *219–221*, 379; d) C. Benelli, D. Gatteschi, *Chem. Rev.* **2002**, *102*, 2369.

[3] a) J.-P. Costes, F. Dahan, A. Dupuis, S. Lagrave, J.-P. Laurent, *Inorg. Chem.* **1998**, *37*, 153; b) J.-P. Costes, F. Nicodème, *Chem. Eur. J.* **2002**, *8*, 3442; c) J.-P. Costes, J. M. Clemente-Juan, F. Dahan, F. Nicodème, *Dalton Trans.* **2003**, 1272; d) N. Ishikawa, T. Iino, Y. Kaizu, *J. Am. Chem. Soc.* **2002**, *124*, 11440; e) T. Gross, F. Chevalier, J. S. Lindsey, *Inorg. Chem.* **2001**, *40*, 4762.

[4] a) R. C. Howell, K. V. N. Spence, I. A. Kahwa, A. J. P. White, D. J. Williams, *J. Chem. Soc. Dalton Trans.* **1996**, 961; b) R. C. Howell, K. V. N. Spence, I. A. Kahwa, D. J. Williams, *J. Chem. Soc. Dalton Trans.* **1998**, 2727; c) M. K. Thompson, M. Vuchkov, I. A. Kahwa, *Inorg. Chem.* **2001**, *40*, 4332; d) D. Sendor, M. Hilder, T. Juestel, P. C. Junk, U. H. Kynast, *New J. Chem.* **2003**, *27*, 1070.

[5] a) P. Guerriero, J.-C. G. Bünzli, E. Moret, *J. Chem. Soc. Dalton Trans.* **1990**, 647; b) K. D. Matthews, S. A. Bailey-Folkes, I. A. Kahwa, G. L. McPherson, C. A. O'Mahoney, S. V. Ley, D. J. Williams, C. J. Groombridge, C. A. O'Connor, *J. Phys. Chem.* **1992**, *96*, 7021; c) P. Froidevaux, J.-C. G. Bünzli, *J. Phys. Chem.* **1994**, *98*; d) J.-C. G. Bünzli, F. Ihringer, *Inorg. Chim. Acta* **1996**, *246*, 195; e) Y. Bretonnière, M. Mazzanti, J. Pécaut, M. M. Olmstead, *J. Am. Chem. Soc.* **2002**, *124*, 9012.

[6] a) R. E. P. Winpenny, *Chem. Soc. Rev.* **1998**, *27*, 447; b) L. Chen, S. R. Breeze, R. J. Rousseau, S. Wang, L. K. Thompson, *Inorg. Chem.* **1995**, *34*, 454; c) S. R. Bayly, Z. Xu, B. O. Patrick, S. J. Rettig, M. Pink, R. C. Thompson, C. Orvig, *Inorg. Chem.* **2003**, *42*, 1576.

[7] a) G. R. Choppin in *Lanthanide Probes in Life, Chemical and Earth Sciences*, (Eds.: J.-C. G. Bünzli, G. R. Choppin), Elsevier, Amsterdam, **1989**, Chapter 1; b) N. Kaltsoyannis, P. Scott, *The f-Elements*, Oxford University Press, **1999**.

[8] D. Chapon, P. Delangle, C. Lebrun, *J. Chem. Soc. Dalton Trans.* **2002**, 68.

[9] a) D. Chapon, C. Husson, P. Delangle, C. Lebrun, P. J. A. Vottéro, *J. Alloys Compd.* **2001**, *323–324*, 128; b) D. Chapon, J.-P. Morel, P. Delangle, C. Gateau, J. Pécaud, *Dalton Trans.* **2003**, 2745.

[10] N. André, R. Scopelliti, G. Hopfgartner, C. Piguet, J.-C. G. Bünzli, *Chem. Commun.* **2002**, 214.
[11] N. André, T. B. Jensen, R. Scopelliti, D. Imbert, M. Elhabiri,G. Hopfgartner, C. Piguet, J.-C. G. Bünzli, *Inorg. Chem.*, DOI 10.1021/ic0351996.
[12] S. Floquet, N. Ouali, B. Bocquet, G. Bernardinelli, D. Imbert, J.-C. G. Bünzli, G. Hopfgartner, C. Piguet, *Chem. Eur. J.* **2003**, *9*, 1860.
[13] a) D.-S. Young, H.-Y. Hung, L. K. Liu, *Rapid Commun. Mass Spectrom.* **1997**, *11*, 769; b) C. A. Schalley, *Int. J. Mass Spectrom.* **2000**, *194*, 11.
[14] a) S. Colette, B. Amekraz, C. Madic, L. Berthon, G. Cote, C. Moulin, *Inorg. Chem.* **2002**, *41*, 7031; b) S. Colette, B. Amekraz, C. Madic, L. Berthon, G. Cote, C. Moulin, *Inorg. Chem.* **2003**, *42*, 2215.
[15] W. Schecher, MINEQL$^+$, version 2.1, MD Environmental Research Software, Edgewater, NJ, **1991**.
[16] N. Ouali, J.-P. Rivera, P.-Y. Morgantini, J. Weber, C. Piguet, *Dalton Trans.* **2003**, 1251.
[17] a) C. F. G. C. Geraldes, C. Piguet in *Handbook on the Physics and Chemistry of Rare Earths, Vol. 33* (Eds.: K. A. Gschneidner, Jr., J.-C. G. Bünzli, V. Pecharsky), Elsevier Science Publishers, Amsterdam, **2003**, Chapter 215; b) J. A. Peters, J. Huskens, D. J. Raber, *Prog. NMR Spectrosc.* **1996**, *28*, 283.
[18] G. Koper, M. Borkovec, *J. Phys. Chem. B* **2001**, *105*, 6666.
[19] M. Borkovec, FITMIX, a programm for the non-linear fit of multimetallic complexation in polyelectrolytes.
[20] S. Petoud, J.-C. G. Bünzli, F. Renaud, C. Piguet, K. J. Schenk, G. Hopfgartner, *Inorg. Chem.* **1997**, *36*, 5750.
[21] a) S. Koeller, G. Bernardinelli, B. Bocquet, C. Piguet, *Chem. Eur. J.* **2003**, *9*, 1062; b) S. Koeller, G. Bernardinelli, C. Piguet, *Dalton Trans.* **2003**, 2395.
[22] R. D. Shannon, *Acta Crystallogr. Sect. A* **1976**, *32*, 751.
[23] a) J. L. Lessmann, W. DeW. Horrocks, Jr., *Inorg. Chem.* **2000**, *39*, 3114; b) J.-C. G. Bünzli, C. Piguet, *Chem. Rev.* **2002**, *102*, 1897.
[24] G. Schwarzenbach, *Complexometric Titrations*, Chapman & Hall, London, **1957**, pp. 8ff.
[25] A. Altomare, M. C. Burla, M. Camalli, G. Cascarano, C. Giacovazzo, A. Guagliardi, A. G. G. Moliterni, G. Polidori, R. Spagna, *J. Appl. Crystallogr.* **1999**, *32*, 115.
[26] XTAL 3.2 User's Manual (Eds.: S. R. Hall, H. D. Flack, J. M. Stewart), Universities of Western Australia and Maryland, **1989**.
[27] C. K. Johnson, ORTEP II, Report ORNL-5138, Oak Ridge National Laboratory, Oak Ridge, TN, **1976**.
[28] J. Rossier, F. Reymond, P. E. Michel, *Electrophoresis* **2002**, *23*, 858.
[29] J. W. Hager, *Rapid Commun. Mass Spectrom.* **2002**, *16*, 512.
[30] R. Rodriguez-Cortinas, F. Avecilla, C. Platas-Iglesias, D. Imbert, J.-C. G. Bünzli, A. de Blas, T. Rodriguez-Blas, *Inorg. Chem.* **2002**, *41*, 5336.

Received: September 1, 2003 [F5498]

